

1 **SYNERGY BETWEEN SATELLITE OBSERVATIONS OF SOIL MOISTURE**
2 **AND WATER STORAGE ANOMALIES FOR RUNOFF ESTIMATION**

3 Stefania Camici ⁽¹⁾, Gabriele Giuliani ⁽¹⁾, Luca Brocca ⁽¹⁾, Christian Massari ⁽¹⁾, Angelica Tarpanelli
4 ⁽¹⁾, Hassan Hashemi Farahani ⁽²⁾, Nico Sneeuw ⁽²⁾, Marco Restano ⁽³⁾, Jérôme Benveniste ⁽⁴⁾

5 *(1) National Research Council, Research Institute for Geo-Hydrological Protection, Perugia, Italy (s.camici@irpi.cnr.it)*

6 *(2) Institute of Geodesy, University of Stuttgart, Geschwister-Scholl-Straße 24D, 70174 Stuttgart, Germany*

7 *(3) SERCO c/o ESA-ESRIN, Largo Galileo Galilei, Frascati, 00044, Italy*

8 *(4) European Space Agency, ESA-ESRIN, Largo Galileo Galilei, Frascati, 00044, Italy*

9

10

11

12

13

14

15

16

17

18

November 2020

19

Submitted to:

20

* Correspondence to: Ph.D. Stefania Camici, Research Institute for Geo-Hydrological Protection, National Research Council, Via della Madonna Alta 126, 06128 Perugia, Italy. Tel: +39 0755014419 Fax: +39 0755014420 E-mail: stefania.camici@irpi.cnr.it.

21 **ABSTRACT**

22 This paper presents an innovative approach, STREAM - SaTellite based Runoff Evaluation And
23 Mapping - to derive daily river discharge and runoff estimates from satellite soil moisture,
24 precipitation and total water storage anomalies observations. Within a very simple model structure,
25 precipitation and soil moisture data are used to estimate the *quick-flow* river discharge component
26 while the total water storage anomalies are used for obtaining its complementary part, i.e., the *slow-*
27 *flow* river discharge component. The two are then summed up to obtain river discharge estimates.

28 The method is tested over the Mississippi river basin for the period 2003-2016 by using Tropical
29 Rainfall Measuring Mission (TRMM) Multi-satellite Precipitation Analysis (TMPA) precipitation
30 data, European Space Agency Climate Change Initiative (ESA CCI) soil moisture data and Gravity
31 Recovery and Climate Experiment (GRACE) total water storage data. Despite the model simplicity,
32 relatively high-performance scores are obtained in river discharge estimates, with a Kling-Gupta
33 efficiency index greater than 0.64 both at the basin outlet and over several inner stations used for
34 model calibration highlighting the high information content of satellite observations on surface
35 processes. Potentially useful for multiple operational and scientific applications, from flood warning
36 systems to the understanding of water cycle, the added-value of the STREAM approach is twofold:
37 1) a simple modelling framework, potentially suitable for global runoff monitoring, at daily time scale
38 when forced with satellite observations only, 2) increased knowledge on the natural processes, human
39 activities and on their interactions on the land.

40

41 Key words: satellite products, soil moisture, water storage variations, conceptual hydrological
42 modelling, rainfall-runoff modelling, Mississippi.

43 1. INTRODUCTION

44 Spatial and temporal continuous river discharge monitoring is paramount for improving the
45 understanding of the hydrological cycle, for planning human activities related to water use as well as
46 to prevent or mitigate the losses due to extreme flood events. To accomplish these tasks, runoff and
47 river discharge data, which represents the aggregated signal of runoff (Fekete et al., 2012), should be
48 available at adequate spatial and temporal resolution. For water resources management and drought
49 monitoring monthly time series over basin area larger than 10'000 km² are sufficient whereas
50 observations up to grid scale of few km and daily or sub-daily time step are required for flood
51 prediction. The accurate spatio-temporally continuous runoff and river discharge estimation at finer
52 spatial or temporal resolution is still a big challenge for hydrologists.

53 Traditional in situ observations of river discharge, even if generally characterized by high temporal
54 resolution (up to sub-hourly time step), typically offer little information on the spatial distribution of
55 runoff within a watershed. Moreover, river discharge observation networks suffer from many
56 limitations such as low station density and often incomplete temporal coverage, substantial delay in
57 data access and large decline in monitoring capacity (Vörösmarty et al., 2002). Paradoxically, this
58 latter issue is exacerbated in developing nations (Crochemore et al., 2020), where the knowledge of
59 the terrestrial water dynamics deserves greater attention due to huge damages to settlements and
60 especially the loss of human lives that occurs regularly.

61 This precarious situation has led to growing interest in finding alternative solutions, i.e., model-based
62 or observation-based approaches, for runoff and river discharge monitoring. Model-based
63 approaches, based on the mathematical description of the main hydrological processes (e.g., water
64 balance models, WBMs, global hydrological models, GHMs, e.g., Döll et al., 2003 or, increasing in
65 complexity, land surface models, LSM, e.g., Balsamo et al., 2009; Schellekens et al., 2017), are able
66 to provide comprehensive information on a large number of relevant variables of the hydrological
67 cycle including runoff and river discharge at very high temporal and spatial resolution (up to hourly

68 sampling and 0.05° grid scale). However, the values of modelled water balance components rely on
69 a massive parameterization of the soil, vegetation and land parameters, which is not always realistic,
70 and are strongly dependent on the GHM or LSM models used, analysis periods (Wisser et al., 2010)
71 and climate forcings selected (e.g. Haddeland et al., 2012; Gudmundsson et al., 2012a, b; Prudhomme
72 et al., 2014; Müller Schmied et al., 2016).

73 Alternatively, the observation-based approaches exploit machine learning techniques and a
74 considerable amount of data to describe the physics of the system (Solomatine and Ostfeld, 2008)
75 with only a limited number of assumptions. Besides being simpler than model-based approaches,
76 these approaches still present some limitations. For example, they rely on a considerable amount of
77 data describing the modelled system's physics and the spatial/temporal extent and the uncertainty of
78 the resulting dataset is determined by both the spatial and temporal coverage and the accuracy of the
79 forcing data (e.g., see E-RUN dataset, Gudmundsson and Seneviratne, 2016; GRUN dataset, Ghiggi
80 et al., 2019; FLO1K dataset, Barbarossa et al., 2018). Additional limitations stem from the employed
81 method to estimate runoff. Indeed, random forests such as employed in Gudmundsson and
82 Seneviratne (2016) like other machine learning techniques, are powerful tools for data driven
83 modeling, but they are prone to overfitting, implying that noise in the data can obscure possible
84 signals (Hastie et al., 2009). Moreover, the influence of land parameters on continental-scale runoff
85 dynamics is not considered as the underlying hypothesis is that the hydrological response of a basin
86 exclusively depends on present and past atmospheric forcing. It is easy to understand that this
87 assumption will only be valid in certain circumstances and might lead to problems, e.g., over complex
88 terrain (Orth and Seneviratne, 2015) or in cases of human river flow regulation (Ghiggi et al., 2019).

89 Remote sensing can provide estimates of nearly all the climate variables of the global hydrological
90 cycle including soil moisture (e.g., Wagner et al., 2007; Seneviratne et al., 2010), precipitation
91 (Huffman et al., 2014) and total terrestrial water storage (e.g., Houborg et al., 2012; Landerer and
92 Swenson, 2012; Famiglietti and Rodell, 2013). It has undeniably changed and improved dramatically
93 the ability to monitor the global water cycle and, hence, runoff. By taking advantage of satellite

94 information, some studies tried to develop methodologies able to optimally produce multivariable
95 datasets from the fusion of in situ and satellite-based observations (e.g., [Rodell et al., 2015](#); [Zhang et](#)
96 [al., 2018](#); [Pellet et al., 2019](#)). Other studies exploited satellite observations of hydrological variables,
97 e.g., precipitation ([Hong et al., 2007](#)), soil moisture ([Massari et al., 2014](#)), and geodetic variables (e.g.,
98 [Sneeuw et al., 2014](#); [Tourian et al., 2018](#)) to monitor single components of the water cycle in an
99 independent way.

100 Although the majority of these studies provide runoff and river discharge data at basin scale and
101 monthly time step, they deserve to be recalled here as important for the purpose of the present study.
102 In particular, [Hong et al. \(2007\)](#) presented a first attempt to obtain an approximate but quasi-global
103 annual streamflow dataset by incorporating satellite precipitation data in a relatively simple rainfall-
104 runoff simulation approach. Driven by the multiyear (1998-2006) Tropical Rainfall Measuring
105 Mission Multi-satellite Precipitation Analysis, runoff was independently computed for each global
106 land surface grid cell through the Natural Resources Conservation Service (NRCS) runoff curve
107 number (CN) method ([NRCS, 1986](#)) and subsequently routed to the watershed outlet to predict
108 streamflow. The results, compared to the in situ observed river discharge data, demonstrated the
109 potential of using satellite precipitation data for diagnosing river discharge values both at global scale
110 and for medium to large river basins. If, on the one hand, the work of [Hong et al. \(2007\)](#) can be
111 considered as a pioneer study, on the other hand it presents a serious drawback within the NRCS-CN
112 method that lacks a realistic definition of the soil moisture conditions of the catchment before flood
113 events. This aspect is not negligible as it is well established that soil moisture is paramount in the
114 partitioning of precipitation into surface runoff and infiltration inside a catchment ([Brocca et al.,](#)
115 [2008](#)). In particular, for the same rainfall amount but different values of initial soil moisture
116 conditions, different flooding effects can occur (see e.g. [Crow et al., 2005](#); [Brocca et al., 2008](#); [Berthet](#)
117 [et al., 2009](#); [Merz and Blöschl, 2009](#); [Tramblay et al., 2010](#)). On this line following [Brocca et al.](#)
118 [\(2009\)](#), [Massari et al. \(2016\)](#) presented a very first attempt to estimate global streamflow data by
119 using satellite Soil Moisture Active and Passive (SMAP, [Entekhabi et al., 2010](#)) and Global

120 Precipitation Measurement (GPM, [Huffman et al., 2019](#)) products. Although the validation was
121 carried out by routing the monthly surface runoff only in a single basin in Central Italy, the obtained
122 results suggested to dedicate additional efforts in this direction.

123 Among the studies that use satellite observations of hydrological variables for runoff estimation, the
124 hydro-geodetic approaches are undoubtedly worth mentioning, see e.g., [Sneeuw et al. \(2014\)](#) for a
125 comprehensive overview or [Lorenz et al. \(2014\)](#) for an analysis of satellite-based water balance
126 misclosures with discharge as closure term. In particular, the satellite mission Gravity Recovery And
127 Climate Experiment (GRACE), which observed the temporal changes in the gravity field, has given
128 a strong impetus to satellite-driven hydrology research ([Tapley et al., 2019](#)). Since temporal gravity
129 field variations over the continents imply water storage change, GRACE was the first remote sensing
130 system to provide observational access to deeper groundwater storage. GRACE and its successor
131 mission GRACE-FO provide monthly snapshots of the Earth's gravity field. The temporal variation
132 is therefore relative to the temporally mean gravity field and, hence, the time variations of water
133 storage are fundamentally relative to the mean storage. This relative water storage variation is termed
134 Total Water Storage Anomaly (TWSA).

135 The relation between GRACE-derived TWSA and runoff was characterized by [Riegger and Tourian](#)
136 [\(2014\)](#), which even allowed the quantification of absolute drainable water storage over the Amazon
137 ([Tourian et al., 2018](#)). In essence, the storage-runoff relation describes the gravity-driven drainage of
138 a basin and, hence, the slow-flow processes. Due to GRACE's spatial-temporal resolution, runoff and
139 river discharge are generally available for large basins ($>160'000 \text{ km}^2$) and at monthly time step.

140 Based on the above discussion, it is clear that each approach presents strengths and limitations that
141 enable or hamper the runoff and river discharge monitoring at finer spatial and temporal resolutions.
142 In this context, this study presents an attempt to find an alternative method to derive daily river
143 discharge and runoff estimates at 0.25° degree spatial resolution exploiting satellite observations and
144 the knowledge of the key mechanisms and processes that act in the formation of runoff, i.e., the role
145 of soil moisture in determining the response of a catchment to precipitation. For that, soil moisture,

146 precipitation and TWSA observations are used as input into a simple modelling framework named
147 STREAM v1.3 (SaTellite based Runoff Evaluation And Mapping, version 1.3, hereafter referred to
148 as STREAM). Unlike classical LSMs, STREAM exploits the knowledge of the system states (i.e.,
149 soil moisture and TWSA) to derive river discharge and runoff, and thus it 1) skips the modelling of
150 the evapotranspiration fluxes which are known to be a non-negligible source of uncertainty (Long et
151 al. 2014), 2) limits the uncertainty associated with the over-parameterization of soil and land
152 parameters and 3) implicitly takes into account processes, mainly human-driven (e.g., irrigation,
153 change in the land use), that might have a large impact on the hydrological cycle and hence on runoff.
154 The detailed description of the STREAM model is given in section 4. The collected datasets and the
155 experimental design for the Mississippi River Basin (section 2) are described in section 3 and 5,
156 respectively. Results, discussion and conclusions are drawn in section 6, 7 and 8, respectively.

157 **2. STUDY AREA**

158 The STREAM model presented here has been tested and validated over the Mississippi River basin
159 (Figure 1a). With a drainage area of about 3.3 million km², the Mississippi River basin is the fourth
160 largest watershed in the world, bordered to the West by the crest of the Rocky Mountains and to the
161 East by the crest of the Appalachian Mountains. According to the Köppen climate classification, the
162 climate is subtropical humid over the southern part of the basin, continental humid with hot summer
163 over the central part, continental humid with warm summer over the eastern and northern parts,
164 whereas a semiarid cold climate affects the western part. The average annual air temperature across
165 the watershed ranges from 4°C in the West to 6°C in the East. On average, the watershed receives
166 about 900 mm/year of precipitation (77% as rainfall and 23% as snowfall), more concentrated in the
167 eastern and southern portions of the basin with respect to its northern and western part (Vose et al.
168 2014).

169 The river flow has a clear natural seasonality mainly controlled by spring snowmelt (coming from
170 the Missouri and the Upper Mississippi, the western and the north-central part of the basin,

171 respectively, [Dyer 2008](#)) and by heavy precipitation exceeding the soil moisture storage capacity
172 (mostly occurring in the eastern and southern part of the basin, [Berghuijs et al., 2016](#)). The basin is
173 also heavily regulated by the presence of large dams (Global Reservoir and Dam Database GRanD,
174 [Lehner et al., 2011](#)) most of them located on the Missouri river and over the Great Plains. In particular,
175 the river reach between Garrison and Gavins Point dams is the portion of the Missouri river where
176 the large main-channel dams have the greatest impact on river discharge providing a substantial
177 reduction in the annual peak floods, an increase on low flows and a reduction on the overall variability
178 of intra-annual discharges ([Alexander et al., 2012](#)). The annual average of Mississippi river discharge
179 at Vicksburg, the outlet river cross-section of the basin, is equal to 17'500 m³/s (see Table 1). Given
180 the variety of climate and topography across the Mississippi River basin, it is a good candidate to test
181 the suitability of the STREAM model for river discharge and runoff simulation.

182 **3. DATASETS**

183 The datasets used in this study include in situ observations, satellite products and runoff verification
184 data. The first two datasets are used as input data to the STREAM model. Conversely, the runoff
185 verification data are used as a benchmark to validate the performance of the STREAM model in
186 simulating the runoff.

187 **3.1 In situ Observations**

188 In situ observations comprise air temperature and river discharge data.

189 For air temperature data the Climate Prediction Center (CPC) Global Temperature data developed by
190 the American National Oceanic and Atmospheric Administration (NOAA) using the optimal
191 interpolation of quality-controlled gauge records of the Global Telecommunication System (GTS)
192 network ([Fan et al., 2008](#)) have been used. The dataset is available on a global regular 0.5°×0.5° grid
193 and provides daily maximum (T_{\max}) and minimum (T_{\min}) air temperature data from 1979 to present
194 (2022). The daily average air temperature data have been generated as the mean of T_{\max} and T_{\min} of
195 each day.

196 Daily river discharge data over the study basin have been taken from the Global Runoff Data Center
197 (GRDC, https://www.bafg.de/GRDC/EN/Home/homepage_node.html). In particular, 11 gauging
198 stations located along the main river network of the Mississippi River basin have been selected to
199 represent the spatial distribution of river discharge over the basin. The location of these gauging
200 stations along with relevant characteristics (e.g., the upstream basin area, the mean annual river
201 discharge and the presence of upstream dams) are summarized in Table 1. Mean annual river
202 discharge ranges from 141 to 17'500 m³/s, and 3 of 11 gages are located downstream of big dams
203 ([Lehner et al., 2011](#)). In particular, gages 1, 2 and 5 are located downstream of Garrison (the fifth-
204 largest earthen dam in the world), Gavins Point and Kanopolis dams, respectively (see Figure 1a and
205 Table 1). The related reservoirs have a maximum storage of 29.383×10⁹ m³, 0.607×10⁹ m³, and
206 1.058×10⁹ m³, respectively.

207 **3.2 Satellite Products**

208 Satellite products include observations of precipitation, soil moisture and TWSA.

209 The satellite precipitation dataset used in this study is the Multi-satellite Precipitation Analysis 3B42
210 Version 7 (her after referred to as TMPA) estimate produced by the National Aeronautics and Space
211 Administration (NASA) as the 0.25°×0.25° quasi-global (50°S-50°N) gridded dataset. The TMPA is
212 a gauged-corrected satellite product, with a latency period of two months, available at 3h sampling
213 interval from 1998 to present. Major details about the *P* dataset, downloadable from
214 <http://pmm.nasa.gov/data-access/downloads/trmm>, can be found in [Huffman et al. \(2007\)](#).

215 Soil moisture data have been taken from the European Space Agency Climate Change Initiative (ESA
216 CCI) Soil Moisture project (<https://esa-soilmoisture-cci.org/>) that provides a surface soil moisture
217 product (referred to first 2–3 cm of soil) continuously updated in terms of spatial-temporal coverage,
218 sensors and retrieval algorithms ([Dorigo et al., 2017](#)). In this study, the daily combined ESA CCI soil
219 moisture product v4.2 is used. It is available at global scale with a grid spacing of 0.25°, for the period
220 1978 to present.

221 TWSA have been obtained from the Gravity Recovery And Climate Experiment (GRACE) satellite
222 mission. Here we employ the NASA Goddard Space Flight Center (GSFC) global mascon model,
223 i.e., Release v02.4, ([Luthcke et al. 2013](#)). It has been produced based on the mass concentration
224 (mascon) approach. The model provides surface mass densities on a monthly basis. Each monthly
225 solution represents the average of surface mass densities within the month, referenced at the middle
226 of the corresponding month. The model has been developed directly from GRACE level-1b K-Band
227 Ranging (KBR) data. It is computed and delivered as surface mass densities per patch over blocks of
228 approximately $1^{\circ} \times 1^{\circ}$ or about $12'000 \text{ km}^2$. Although the mascon size is smaller than the inherent
229 spatial resolution of GRACE of about $2.5^{\circ} \times 2.5^{\circ}$ or $64'000 \text{ km}^2$ ([Vishwakarma et al., 2018](#)), the model
230 exhibits a relatively high spatial resolution. This is attributed to a statistically optimal Wiener
231 filtering, which uses signal and noise full covariance matrices. This allows the filter to fine tune the
232 smoothing in line with the signal-to-noise ratio in different areas. That is, the less smoothing, the
233 higher signal-to-noise ratio in a particular area and vice versa. This ensures that the filtering is
234 minimal and aggressive smoothing is avoided when unnecessary. Further details of such a filter can
235 be found in [Klees et al. \(2008\)](#). Importantly, the coloured noise characteristic of KBR data was taken
236 in to account when compiling the GRACE model, which has allowed for a reliable computation of
237 the aforementioned noise full covariance matrices. The coloured noise characteristic of KBR data
238 was taken into account when compiling the model, which has allowed for a reliable computation of
239 these noise and signal covariance matrices. They play a crucial role when filtering and allow a higher
240 spatial resolution compared to commonly applied GRACE filtering methods such as Gaussian
241 smoothing and/or destriping filters. The GRACE data used here are available from January 2003 to
242 July 2016, which suffices to demonstrate the STREAM capabilities. With its successor mission
243 GRACE Follow-On (GRACE-FO), launched early 2018, the time series of time-variable gravity has
244 reached a nearly uninterrupted time span of about 20 years, thus allowing a continued and operational
245 use of STREAM. The existing interruptions, short ones due to mission operations or technical

246 failures, but also the one-year gap between GRACE and GRACE-FO can be dealt with in various
247 ways, e.g. by data driven gap filling (Yi and Sneeuw, 2021).

248 **3.3 Runoff Verification Data**

249 To establish the quality of the STREAM model in runoff simulation, monthly runoff data obtained
250 from the Global Runoff Reconstruction (GRUN_v1, <https://doi.org/10.3929/ethz-b-000324386>) have
251 been used for comparison. The GRUN dataset (Ghiggi et al., 2019) is a global monthly runoff dataset
252 derived through the use of a machine learning algorithm trained with in situ river discharge
253 observations of relatively small catchments (<2500 km²) and gridded precipitation and temperature
254 derived from the Global Soil Wetness Project Phase 3 (GSWP3) dataset (Kim et al., 2017). The
255 dataset covers the period from 1902 to 2014 and it is provided on a 0.5° × 0.5° regular grid.

256 **4. METHOD**

257 **4.1 STREAM Model: the Concept**

258 The STREAM model conceives river discharge as a combination of hydrological responses operating
259 at diverse time scales (Blöschl et al., 2013; Rakovec et al., 2016). In particular, river discharge can
260 be considered made up of a *slow-flow* component, produced as outflow of the groundwater storage
261 and of a *quick-flow* component, i.e. mainly related to the surface and shallow-subsurface runoff
262 components (Hu and Li, 2018).

263 While the high spatial and temporal variability of precipitation and the highly changing land cover
264 spatial distribution significantly impact the variability of the *quick-flow* river discharge component
265 (with scales ranging from hours to days and metres to kilometres depending on the basin size), *slow-*
266 *flow* river discharge reacts to precipitation inputs more slowly as water infiltrates, is stored, mixed
267 and is eventually released in times spanning from weeks to months. Therefore, the two components
268 can be estimated by relying upon two different approaches that involve different types of
269 observations. Based on that, within the STREAM model, satellite soil moisture, precipitation and
270 TWSA will be used for deriving river discharge and runoff estimates. The first two variables are used

271 as proxy of the *quick-flow* river discharge component while TWSA is exploited for obtaining its
272 complementary part, i.e., the *slow-flow* river discharge component. Firstly, we exploit the role of the
273 soil moisture in determining the response of the catchment to the precipitation inputs, which have
274 been soundly demonstrated in more than ten years of literature studies (see e.g., [Brocca et al., 2017](#)
275 for a comprehensive discussion on the topic). Secondly, we consider the important role of total water
276 storage in determining the *slow-flow* river discharge component as modelled in several hydrological
277 models (e.g., [Sneeuw et al., 2014](#)).

278 It is worth noting that modeling the *quick-flow* and *slow-flow* river discharge components
279 independently has been largely applied and tested in recent and past studies, e.g., for the estimation
280 of the flow duration curve (see e.g., [Botter et al., 2007a, b](#); [Yokoo and Sivapalan 2011](#); [Muneepeerakul](#)
281 [et al., 2010](#); [Ghotbi et al., 2020](#)).

282 **4.2 STREAM Model**

283 The STREAM model is a semi-distributed conceptual hydrological model that uses gridded satellite-
284 derived inputs of precipitation, soil moisture, TWSA and air temperature to estimate daily values of
285 gridded runoff and river discharge time series at select basin outlets.

286 To set up the model, the catchment is divided into b sub-catchments, each one representing either a
287 tributary draining area with outlet along the main channel or an area draining directly into the main
288 channel (see Figure 2). Each sub-catchment, assumed homogeneous, is further divided into an array
289 N_b of individual cells assumed as the unit basis for the runoff generation. Note that the number N_b
290 differs for each sub-catchment as, for a fixed cell grid size, it varies with the sub-catchment area.
291 Once estimated at cell scale and aggregated at the sub-basin scale (see section 4.2.1 for details), the
292 runoff is routed at each sub-catchment outlet (see section 4.2.2) and then transferred through the
293 channels and the rivers for the computation of the river discharge at intermediate outlets or at the
294 outlet of the entire basin (see section 4.2.3).

295 Based on that, hereinafter we refer to river discharge, Q , to indicate the amount of water passing a
296 particular point of a river (in $\text{m}^3 \text{s}^{-1}$) whereas runoff, R , is regarded as the depth of water produced
297 from a drainage area during a particular time interval (in mm). The difference between the two
298 quantities is related to the routing processes that allow to transform the runoff into river discharge.

299 **4.2.1 Runoff generation at cell scale**

300 The soil zone of each cell i of the basin is divided into two layers, the upper and lower soil storages
301 allowing to model the related runoff responses, $R_{q,i}$ [mm] and $R_{s,i}$ [mm], as illustrated in Figure 2b.

302 The upper cell storage receives inputs from precipitation (P_i), released through a snow module
303 (Cislaghi et al., 2020) as rainfall (r_i) or stored as snow water equivalent (SWE_i) within the snowpack
304 and on the glaciers. In particular, according to Cislaghi et al. (2020), SWE_i is modelled by using as
305 input air temperature ($T_{\text{air},i}$) and a degree-day coefficient, C_m , to be estimated by calibration.

306 Once precipitation is partitioned by the snow model, the rainfall output r_i contributes to $R_{q,i}$ while the
307 SWE_i (like other fluxes contributing to modify the soil water content into Su) is neglected as already
308 considered in the satellite TWSA. Therefore, the first key point of the STREAM model is that the
309 water content in the upper storage of soil zone, Su (Figure 2b), is directly provided by the satellite
310 soil moisture observations and the loss processes like percolation or evaporation do not need to be
311 explicitly modelled to estimate the evolution in time of soil moisture. Consequently, for each cell i ,
312 $R_{q,i}$ can be computed following the formulation proposed by Georgakakos and Baumer (1996), as in
313 equation (1):

$$314 \quad R_{q,i}(t) = r_i(t) SWI_i(t, T)^\alpha \quad (1)$$

315 where:

316 - t [days] represents the time;

317 - r_i [mm] is the rainfall, obtained as an output from the snow module;

318 - SWI_i [-] is the Soil Water Index (Wagner et al., 1999), i.e., the root-zone soil moisture product
 319 referred to the first layer of the model (representative of the first 5–30 cm of soil), derived by the
 320 surface satellite soil moisture product, θ_i , by applying the exponential filtering approach in its
 321 recursive formulation (Albergel et al., 2009):

$$322 \quad SWI_{i,n} = SWI_{i,n-1} + K_n(\theta_i(t_n) - SWI_{i,n-1}) \quad (2)$$

323 with the gain K_n at the time t_n given by:

$$324 \quad K_n = \frac{K_{n-1}}{K_{n-1} + e^{\left(\frac{t_n - t_{n-1}}{T}\right)}} \quad (3)$$

325 - T [days] is a parameter, named characteristic time length, that characterizes the temporal variation
 326 of soil moisture within the root-zone profile and the gain K_n ranges between 0 and 1;

327 - α [-] is a coefficient linked to the non-linearity of the infiltration process and it considers the
 328 characteristics of the soil;

329 - for the initialization of the filter $K_1 = 1$ and $SWI_1 = \theta(t_1)$.

330 The second key point of STREAM model concerns the estimation of $R_{s,i}$, i.e., the *slow-runoff* response
 331 related to the lower storage of the soil zone. The hypothesis here, shared also with other studies (e.g.,
 332 Rakovec et al., 2016), is that the dynamic of R_s can be represented by the monthly TWSA data. Indeed,
 333 the time scale of R_s is typically in the range of seasons to years and it can be assumed almost
 334 independent of the water that is contained in the upper storage. For that, for each cell i , $R_{s,i}$ can be
 335 computed following the formulation proposed by Famiglietti and Wood (1994), through equation (4)
 336 as follows:

$$337 \quad R_{s,i}(t) = \beta (TWSA_i^*(t))^m \quad (4)$$

338 where:

339 - $TWSA_i^*$ [-] is the TWSA estimated by GRACE over the cell i normalized by its minimum and
 340 maximum values. The assumption behind this equation is that TWSA can be assumed as a proxy
 341 of the evolution in time of the Sl , i.e., the water amount in the lower storage of the soil zone.
 342 - β [mm h^{-1}] and m [-] are two parameters describing the nonlinearity between lower storage runoff
 343 component and $TWSA^*$.

344 Note that we made the hypothesis that soil moisture and TWSA observations are independent
 345 (whereas in reality soil moisture can be responsible both for the generation of R_q (mainly) and for the
 346 R_s contribution) given the different temporal (and spatial) scales at which the upper and lower runoff
 347 responses act.

348 By neglecting any lateral flow, the runoff responses at cell scale are averaged at sub-catchment scale
 349 to obtain b runoff responses, one for each sub-catchment. Specifically, by considering N_b cells for
 350 each sub-catchment, the following equation are used:

$$351 \quad R_{q,b}(t) = \frac{\sum_{i=1}^{N_b} R_{q,i}(t)}{N_b} \quad (5)$$

$$352 \quad R_{s,b}(t) = \frac{\sum_{i=1}^{N_b} R_{s,i}(t)}{N_b} \quad (6)$$

353 **4.2.2 Sub-catchment river discharge calculation**

354 For each sub-catchment b , the runoff component $R_{q,b}$ is routed to its outlet by the Geomorphological
 355 Instantaneous Unit Hydro-graph (GIUH, [Gupta et al., 1980](#)) for tributary draining areas or through a
 356 linear reservoir approach ([Nash, 1957](#)) for directly draining areas. The $R_{s,b}$ runoff component is
 357 transferred to the sub-catchment outlet by a linear reservoir approach. These processes are controlled
 358 by a parameter lag time, L [days], evaluated as ([Corradini et al., 2002](#)):

$$359 \quad L = \gamma 1.19 A_b^{0.33} \quad (7)$$

360 where A_b [km^2] is the sub-catchment area and γ [-] is a parameter to be calibrated.

361 By routing the $R_{q,b}$ and $R_{s,b}$ components the *quick-flow*, $Q_{q,b}$ [m³/s], and the *slow-flow*, $Q_{s,b}$ [m³/s]
362 river discharge components at each sub-catchment outlet are obtained (see Figure 2c).

363 **4.2.3 River discharge routing through river networks**

364 A diffusive linear approach (controlled by the parameters C [km h⁻¹] and D [km² h⁻¹], i.e., Celerity
365 and Diffusivity, Troutman and Karlinger, 1985) is applied to route the two river discharge
366 components, $Q_{q,b}$ and $Q_{s,b}$ through the river network from the sub-catchment outlet to intermediate
367 outlets along the river or to the outlet of the entire basin (Brocca et al., 2011). In this way the *quick-*
368 *flow*, Q_q [m³/s], and the *slow-flow*, Q_s [m³/s] river discharge components at the catchment outlet are
369 obtained (see Figure 2d).

370 **4.3 STREAM Parameters**

371 The STREAM model uses 8 calibration parameters for each sub-catchment b into which the entire
372 basin is divided. Among these parameters, 5 control the runoff generation process (α , T , β , m , C_M)
373 and 3 the routing component and therefore the streamflow dynamics (γ , C and D). The parameter
374 values determined within the feasible parameter space (See Table Appendix A for more details), are
375 calibrated by maximizing the Kling-Gupta Efficiency index (***KGE***, Gupta et al., 2009; Kling et al.,
376 2012, see section 5.1 for more details) between observed and modelled river discharge. For model
377 calibration, a standard gradient-based automatic optimisation method (Bober 2013) was used.

378 **5. EXPERIMENTAL DESIGN**

379 **5.1 Modelling Setup for Mississippi River Basin**

380 The modelling setup is carried out in three steps (Figure 3):

381 1. *Sub-catchment delineation*. The TopoToolbox (<https://topotoolbox.wordpress.com/>), a tool
382 developed in Matlab by Schwanghart and Kuhn (2010), and the SHuttle Elevation Derivatives at
383 multiple Scales (HydroSHED, <https://www.hydrosheds.org/>) DEM of the basin at the 3'' resolution
384 (nearly 90 m at the equator) have been used to derive flow directions, to extract the stream network

385 and to delineate the drainage basins over the Mississippi River basin. In particular, by considering
386 only rivers with order greater than 3 (according to the Horton-Strahler rules, Horton, 1945; Strahler,
387 1952), the Mississippi watershed has been divided into 53 sub-catchments as illustrated in Figure 1a.
388 Blue lines in the figure illustrate the river network pathway connecting the sub-catchments, red dots
389 indicate the location of the 11 river discharge gauging stations selected for the study area.

390 It has to be specified that the step of sub-basin delineation could be accomplished through tools
391 different from the TopoToolbox. For instance, it could be used the free Qgis software downloadable
392 at <https://www.qgis.org/it/site/forusers/download.html>, following the instruction to perform the
393 hydrological analysis as in
394 [https://docs.qgis.org/3.16/en/docs/training_manual/processing/hydro.html?highlight=hydrological%](https://docs.qgis.org/3.16/en/docs/training_manual/processing/hydro.html?highlight=hydrological%20analysis)
395 [20analysis](https://docs.qgis.org/3.16/en/docs/training_manual/processing/hydro.html?highlight=hydrological%20analysis).

396 *2. Extraction of input data.* Precipitation, air temperature, soil moisture and TWSA datasets data have
397 to be extracted for each sub-catchment of the study area. If characterized by different spatial/temporal
398 resolution, these datasets need to be resampled over a common spatial grid/temporal time step prior
399 to be used as input into the model.

400 To run the STREAM model over the Mississippi river basin, input data have been resampled over the
401 precipitation spatial grid at 0.25° resolution through a bilinear interpolation. Concerning the temporal
402 scale, air temperature, soil moisture and precipitation data are available at daily time step, while
403 monthly TWSA data have been linearly interpolated at daily time step. For each of the 53 Mississippi
404 sub-catchment, the resampled precipitation, soil moisture, air temperature and TWSA data have been
405 extracted (see Figure 1b and 1c).

406 *3. STREAM model calibration.* In situ river discharge data are used as reference data for the
407 calibration of STREAM model. For Mississippi, the STREAM model has been calibrated at five
408 gauging stations, i.e., the stations 4, 6, 9, 11 and 10. This allowed to identify five sets of STREAM
409 parameters attributed to each catchment according to the river network pathway illustrated in Figure
410 1a. This means that, for example, to the sub-catchments labelled as 1, 2, 5 to 15, 17, 22, 23, and 30

411 contributing to the gauging station 4 are attributed the parameter set obtained by calibrating the model
412 against river discharge data observed at station 4; to the sub-catchments 31, 37, 38 and 41 contributing
413 to gauging station 6 are attributed the parameter set obtained by calibrating the model with respect to
414 gauging station 6 and so on. Consequently, the sub-catchments highlighted with the same colour in
415 Figure 1a are assigned the same model parameters, i.e. the parameters that allow to reproduce the
416 river discharge data observed at the related gage.

417 Once calibrated, the STREAM model has been run to provide continuous daily runoff and river
418 discharge time series, over each grid pixel and at the outlet section of each sub-catchment,
419 respectively. By considering the spatial/temporal availability of both in situ and satellite observations,
420 the entire analysis period covers the maximum common observation period, i.e., from January 2003
421 to July 2016 at daily time scale. To establish the goodness-of-fit of the model, the modelled river
422 discharge and runoff timeseries are compared against in situ river discharge and modelled runoff data.

423 **5.2 Model Evaluation Criteria and Performance Metrics**

424 The model has been run over a 13.5-year period split into two sub periods: the first 8 years, from
425 January 2003 to December 2010, are used to calibrate the model. The model is validated, as described
426 below over the remaining 5.5 years (January 2011 - July 2016).

427 In particular, three different validation schemes have been adopted to assess the robustness of the
428 STREAM model:

- 429 1. internal validation aimed to test the plausibility of both the model structure and the parameter set
430 in providing reliable estimates of the hydrological variables against which the model is calibrated.
431 For this purpose, a comparison between observed and modelled river discharge time series on the
432 gauging stations used for model calibration has been carried out for both the calibration and
433 validation sub periods;
- 434 2. cross-validation testing the goodness of the model structure and the calibrated model parameters
435 to predict hydrological variables at locations not considered in the calibration phase. In this

436 respect, the cross-validation has been carried out by comparing observed and modelled river
 437 discharge time series in gauging stations not considered during the calibration phase;

438 3. external validation aimed to test the capability of the model “*to get the right answers for the right*
 439 *reasons*” (Kirchner 2006). The rationale behind this concept is that the hydrological models are
 440 today highly performing and able to reproduce a lot of hydrological variables. For that, the model
 441 performances should not only be evaluated against observed river discharge, but complementary
 442 datasets representing internal hydrologic states and fluxes (e.g., soil moisture, evapotranspiration,
 443 runoff etc) should be considered. As runoff is a secondary product of the STREAM model,
 444 obtained indirectly from the calibration of the river discharge (basin-integrated runoff), the
 445 comparison in terms of runoff can be considered as a further external validation of the model.
 446 Runoff, differently from river discharge, cannot be directly measured. It is generally modelled
 447 through land surface or hydrological models. Its validation requires a comparison against
 448 modelled data that, however, suffer from uncertainties (Beck et al., 2017). Based on that, in this
 449 study the GRUN runoff dataset described in the section 3.3 has been used for a qualitative
 450 comparison.

451 5.3 Performance Metrics

452 To measure the goodness-of-fit between modelled and observed river discharge data three
 453 performance scores have been used:

- 454 • the root mean square error relative to the mean, *RRMSE*:

$$455 \text{ RRMSE} = \frac{\sqrt{\frac{1}{n} \sum_{j=1}^n (Q_{modj} - Q_{obsj})^2}}{\frac{1}{n} \sum_{j=1}^n (Q_{obsj})} \quad (8)$$

456 where Q_{obs} and Q_{mod} are the observed and modelled river discharge time series of length n . *RRMSE*
 457 values range from 0 to $+\infty$, the lower the *RRMSE*, the better the agreement between observed and
 458 modelled data.

- 459 • the Pearson correlation coefficient, *rho*, measuring the linear relationship between two variables:

460
$$rho = \frac{\sum_{j=1}^n (Q_{modj} - \overline{Q_{mod}})(Q_{obsj} - \overline{Q_{obs}})}{\sqrt{\sum_{j=1}^n (Q_{modj} - \overline{Q_{mod}})^2 (Q_{obsj} - \overline{Q_{obs}})^2}} \quad (9)$$

461 where $\overline{Q_{obs}}$ and $\overline{Q_{mod}}$ represent the mean values of Q_{obs} and Q_{mod} , respectively. The values of rho
 462 range between -1 and 1 ; higher values of R indicate a better agreement between observed and
 463 modelled data.

- 464 • the Kling-Gupta efficiency index (*KGE*, Gupta et al., 2009), which provides direct assessment of
 465 four aspects of river discharge time series, namely shape, timing, water balance and variability.

466 It is defined as follows:

467
$$KGE = 1 - \sqrt{(rho - 1)^2 + (\delta - 1)^2 + (\varepsilon - 1)^2} \quad (10)$$

468 where δ is the relative variability and ε the bias normalized by the standard deviation between
 469 observed and modelled river discharge. The *KGE* values range between $-\infty$ and 1 ; the higher the *KGE*
 470 the better is the agreement between observed and modelled data. Simulations characterized by values
 471 of *KGE* in the range -0.41 and 1 can be assumed as reliable; values of *KGE* greater than 0.5 have been
 472 assumed good with respect to their ability to reproduce observed time series (Thiemig et al., 2013).

473 **5.4 STREAM sensitivity analysis**

474 To investigate how the variation of the STREAM parameters influences the variation of the STREAM
 475 model outputs, a global sensitivity analysis has been carried out. Specifically, the Variance-Based
 476 sensitivity analysis (VBSA, Sobol 1993) implemented into the Sensitivity Analysis For Everybody
 477 toolbox (SAFE, Pianosi et al., 2015, <https://www.safetoolbox.info/>) has been applied. VBSA relies
 478 on the variance decomposition and consists of assessing the contributions to the variance of the model
 479 output from variations in the parameters. In this study, we use as sensitivity index the first-order (main
 480 effect) index, which measures the variance contribution from variations in an individual input factor
 481 alone (i.e., excluding interactions with other factors) and the total sensitivity indices, which measure
 482 the total contribution of a single input factor or a group of inputs including interactions with all other
 483 inputs. The following steps were carried out to execute the VBSA. Firstly, the locality-sensitive

484 hashing (LSH) technique was used to generate 15000 samples from the model parameter space (see
485 Table 1A). Previous hydrological studies (e.g., [Tang et al., 2007](#)) recommend the LHS sampling
486 method for its sampling efficiency. Secondly, 15000 STREAM model runs were executed and the
487 corresponding *KGE* values (11x15000 values, one for each gauging station for each run) were
488 retained. Thirdly, the parameters and the 15000 *KGE* samples were used in the SAFE toolbox to
489 compute the sensitivity indices.

490 For major details on the workflow needed to implement the VBSA the reader is referred to [Noacco](#)
491 [et al. \(2020\)](#).

492 **6. RESULTS**

493 The testing and validation of the STREAM model is presented and discussed in this section according
494 to the scheme illustrated in section 5.2.

495 **6.1 Internal Validation**

496 The performance of the STREAM model over the gauging stations used for calibration is illustrated
497 in Figure 4 and summarized in Table 2. Figure 4 shows observed and modelled river discharge time
498 series over the whole study period (2003-2016); in Table 2 the performance scores are evaluated
499 separately for the calibration and validation sub periods. It is worth noting that the model accurately
500 predicts the observed river discharge data and is able to give the “right answer” with good modelling
501 performances. Score values of *KGE* and *rho* over the calibration period are higher than 0.78 for all
502 the calibrated gauging stations; *RRMSE* is lower than 45% for all the calibrated gauging stations
503 except for station 9, where it rises up to 66%. The performances remain good even if they are
504 evaluated over the validation period or the entire study period as indicated by the scores on the top of
505 each plot of Figure 4.

506 **6.2 Cross-validation**

507 The cross-validation has been carried out over the six gauging stations illustrated in Figure 5 not used
508 in the calibration step. The performance scores on the top of each plot refer to the entire study periods;

509 the scores split for calibration and validation periods are reported in Table 2. For some river discharge
510 gauging stations the performance is quite low (see, e.g., gauging station 1, 2 and 5) whereas for others
511 the model is able to estimate river discharge data quite accurately (e.g., 7 and 8). In particular, for the
512 gauging stations 1 and 2 even if *KGE* reaches values equal to 0.39 and 0.46 for the whole period,
513 respectively, there is not a good agreement between observed and modelled river discharge and the
514 *rho* score is lower than 0.56 for both the stations. The worst performance is obtained over the gauging
515 station 5, with negative *KGE* and low *rho* values. These results are certainly influenced by the
516 presence of large dams located upstream to these stations (i.e., Garrison, Gavins Point and Kanopolis
517 dams, see Table 1) which have a strong impact on river discharge: the model, not having a specific
518 module for modelling reservoirs, is not able to accurately reproduce the dynamics of river discharge
519 over regulated river stations. Positive *KGE* values are obtained over the gauging stations 3, 7 and 8.
520 In particular, over the gauging station 3 the STREAM model overestimates the observed river
521 discharge due the presence of large dams along the Missouri river, over the Great Plains region. This
522 area is well known from other large-scale hydrological models (e. g., ParFlow-CLM and WRF-
523 Hydro) to be an area with very low performances in terms of river discharge modelling (O'Neill et
524 al., 2020, Tijerina et al., 2021).

525 Over the gauging station 7, located over the Rock river, a relatively small tributary of the Mississippi
526 river (see Table 1), the STREAM model overestimation has to be attributed to: 1) the different
527 characteristics of the Rock river basin with respect to the entire basin closed to station 6 where the
528 model has been calibrated (see Figure 1a); 2) the small size of the Rock river basin (23'000 km², if
529 compared with GRACE resolution, 160'000 km²) for which the model accuracy is expect to be lower.
530 Conversely, the performances over the gauging station 8, whose parameters have been set equal to
531 the ones of gauging station 10, are quite high (*KGE* equal to 0.71, 0.81 and 0.78 for the entire, the
532 calibration and the validation period, respectively; *rho* equal to 0.82, 0.84 and 0.83 for the entire,
533 calibration and validation periods, respectively). This outcome demonstrates that under some

534 circumstances, the STREAM model can be used to estimate river discharge in basins not calibrated
535 over, especially those without upstream dams and with comparable size and land cover.

536 On overall, the cross-validation results suggest that the performances of STREAM model, as any
537 hydrological model calibrated against observed data, decrease over the gauging stations not used for
538 the calibration raising doubts about the robustness of model parameters and whether it is actually
539 possible to transfer model parameters from one river section to another with different inter-basin
540 characteristics. A more in-depth investigation about the model calibration procedure, with special
541 focus on the regionalization of the model parameters, should be carried out but this topic is beyond
542 the scope of the manuscript.

543 **6.3 External Validation**

544 For the external validation, the monthly runoff time series provided by the GRUN datasets have been
545 compared against the ones computed by the STREAM model. For that, STREAM daily runoff time
546 series have been aggregated at monthly scale and re-gridded at the same spatial resolution of the
547 GRUN dataset (0.5°). The comparison is illustrated in Figure 6 for the common period 2003–2014.
548 Although the two datasets consider different precipitation inputs, the two models agree in identifying
549 two distinct zones in terms of runoff, i.e., the western dry and the eastern wet area. These two distinct
550 zones can be clearly identified also in the GSWP3 and TMPA 3B42 V7 precipitation maps (see Figure
551 A1) used as input in GRUN and STREAM, respectively, stressing that STREAM runoff output is
552 correctly driven by the input data. However, likely due to the calibration procedure, the STREAM
553 runoff map appears patchier with respect to GRUN and discontinuities along the sub-basin boundaries
554 (identified in Figure 1a) can be noted. This should be ascribed to the automatic calibration procedure
555 of the model that, differently from other calibration techniques (e. g., regionalization procedures),
556 does not consider the basin physical attributes like soil, vegetation, and geological properties that
557 govern spatial dynamics of hydrological processes. This calibration procedure can generate sharp
558 discontinuities even for neighbouring sub-catchments individually calibrated. It leads to

559 discontinuities in model parameter values and consequently in the modelled hydrological variable
560 (runoff).

561 **6.4 Sensitivity analysis results**

562 The results of the VBSA, are illustrated in Figure 7a in terms of main effect indices and in Figure 7b
563 in terms of total effect. Specifically, the figure refers to Vicksburg station but similar results have
564 been obtained for all the 11 gauging stations in the Mississippi basin. By looking at Figure 7, we
565 observe that the model parameters most influencing the model response are β and m , i.e., the two
566 parameters controlling the *slow-flow* runoff response of the lower soil storage. In particular, the total
567 effect sensitivity index of these two parameters is higher than the main effect sensitivity index. This
568 means that these two parameters have an effect on the model output not only through their individual
569 variations but also through interactions with other parameters. Instead, the other five parameters (α ,
570 T , γ , C , D and C_m) have low main and total effect indices, and consequently, these parameters have
571 a small effect, both direct and through interactions, on model response. Among these, only the
572 α parameter shows a slightly high main and total effect sensitivity indices.

573 This outcome is very important as it allows to clearly distinguish model parameters which values
574 should be carefully determined when calibrating the model (β and m and partially α) from the least
575 sensitive (T , γ , C , D and C_m) which values could be set values within the model parameters' range of
576 variability and then excluded during the calibration phase.

577 **7. DISCUSSION**

578 In the previous sections, the ability of the STREAM model to estimate river discharge and runoff
579 time series has been presented. In particular, Figures 4, 5 and 6 demonstrate that satellite observations
580 of precipitation, soil moisture and total water storage anomalies can provide accurate daily river
581 discharge estimates for near-natural large basins (absence of upstream dams), and for basins with
582 draining area greater than 160'000 km² (see section 6.2), i.e., at spatial/temporal resolution greater

583 than the ones of the TWSA input data (monthly, 160'000 km²). This is an important result of the
584 study as it demonstrates, on one hand, that the model structure is appropriate with respect to the data
585 used as input and, on the other hand, the great value of information contained into TWSA data that,
586 even if characterized by limited spatial/temporal resolution, can be used to estimate runoff and river
587 discharge at basin scale. This finding has been also confirmed by a preliminary sensitivity analysis in
588 which the STREAM model has been run with different hydrological inputs of precipitation, soil
589 moisture and total water storage anomaly (not shown here for brevity). In particular, by running the
590 STREAM model with different input configurations (e.g., by using TMPA 3B42 V7 or CPC data for
591 precipitation, ESA CCI or Advanced SCATterometer (ASCAT) data for soil moisture, TWSA or ESA
592 CCI soil moisture data to model the slow-flow river discharge component), we found that STREAM
593 results are more sensitive to soil moisture data rather than to precipitation input. In addition, by
594 running STREAM model with soil moisture data as input to model the slow-flow river discharge
595 component (i.e. without using TWSA data) we found a deterioration of the model results. This
596 outcome along with the one obtained in the section 6.3, demonstrating the high sensitivity of the
597 model parameters related to *slow-flow* river discharge component, confirm the paramount role of
598 TWSA in estimating river discharge. In this respect, the availability of GRACE data up to July 2016
599 could represent an issue for the model application beyond that date. However, the GRACE-FO along
600 with the numerous literature studies devoted to fill the GRACE data gap between GRACE and
601 GRACE-FO (see e.g., [Landerer et al., 2020](#) or [Yi and Sneeuw, 2021](#)), can provide the needed data to
602 extend the STREAM model application up to present. Further developments in this direction are
603 expected with the ESA's Next Generation Gravity Mission (NGGM), a candidate Mission of
604 Opportunity for ESA–NASA cooperation in the frame of the Mass Change and Geosciences
605 International Constellation (MAGIC) that will enable long-term monitoring of the temporal variations
606 of Earth's gravity field at relatively high temporal (down to 3 days) and increased spatial resolutions
607 (up to 100 km). This implies also that time series of GRACE and GRACE-FO can be extended
608 towards a climate series ([Massotti et al., 2021](#)).

609 By looking at technical reviews of large-scale hydrological models (e.g., Sood and Smakhtin, 2015,
610 Kauffeldt et al., 2016), it can be noted there are many established models, similar in objective and
611 limitations to STREAM model, already existing with support and user base (e.g., among others,
612 Community Land Model, CLM, Oleson et al., 2013; European Hydrological Predictions for the
613 Environment, E-HYPE, Lindström et al., 2010; H08, Hanasaki et al., 2008, PCR-GLOBWB, van
614 Beek and Bierkens, 2008; Water – a Global Assessment and Prognosis WaterGAP, Alcamo et al.,
615 2003; ParFlow–CLM, Maxwell et al., 2015; WRF-Hydro, Gochis et al., 2018; Precipitation-Runoff
616 Modeling System, PRMS; Markstrom et al., 2015). Some of them, e.g., ParFlow-CLM, WRF-Hydro
617 or PRMS have been specifically configured across the continental United States and showed good
618 capability to reproduce observed streamflow data over the Mississippi river basin with performances
619 decreased throughout the Great Plains (O'Neill et al., 2020, Tijerina et al., 2021) which is consistent
620 with the results we obtained with the STREAM model. However, with respect to classical
621 hydrological and land surface models, STREAM is based on a new concept for estimating runoff and
622 river discharge which relies on the almost exclusive use of satellite observations, and, a simplification
623 of the processes being modelled.

624 This approach brings several advantages: 1) satellite data implicitly consider the human impact on
625 the water cycle observing some processes, such as irrigation application or groundwater withdrawals,
626 that are affected by large uncertainty in classical hydrological models, 2) the satellite technology
627 grows quickly and hence it is expected that the spatial/temporal resolution and accuracy of satellite
628 products will be improved in the near future (e.g., 1 km resolution from new satellite soil moisture
629 products and the next generation gravity mission); the STREAM model is able to fully exploit such
630 improvements; 3) STREAM model models only the most important processes affecting the
631 generation of runoff, and considers only the most important variables as input (precipitation, surface
632 soil moisture and groundwater storage). In other words, the model does not need to parametrize
633 processes, such as evapotranspiration and percolation and therefore it is an independent modelling

634 approach for simulating runoff and river discharge that can be also exploited for benchmarking and
635 improving classical land surface and hydrological models.

636 **7.1 Strengths and limitations of STREAM model**

637 Hereinafter, the strengths and the main limitations of the STREAM model are discussed.

638 Among the strengths of the STREAM model it is worth highlighting:

639 **Simplicity.** The STREAM model structure: 1) limits the input data required. Only precipitation, air
640 temperature, soil moisture and TWSA data are needed as input whereas LSM/GHMs require many
641 additional inputs such as wind speed, shortwave and longwave radiation, pressure and relative
642 humidity; 2) limits and simplifies the processes to be modelled for runoff and river discharge
643 simulation. Processes like evapotranspiration or percolation, are not modelled therefore avoiding the
644 need of using sophisticated and highly parameterized equations (e.g., Penman-Monteith for
645 evapotranspiration, Allen et al.,1998); 3) limits the number of parameters (only 8 parameters have to
646 be calibrated) thus simplifying the calibration procedure and potentially reduces the model
647 uncertainties related to the estimation of parameter values.

648 In particular, the STREAM model is even simpler than the classical semi-distributed conceptual
649 hydrological models available in literature. As an example, for the comparison we could refer to the
650 Hydrologiska Byråns Vattenbalansavdelning model (HBV, Bergström 1995) or to the Hydrologic
651 Engineering Center – Hydrologic Modeling System (HEC-HMS, Feldman, 2000). HBV model counts
652 14 parameters to be calibrated and needs precipitation, air temperature and potential
653 evapotranspiration as input data. Similar input data are required for HEC-HMS which counts 23
654 parameters. Both the models, uses conceptual equations to estimate the soil losses and to model the
655 soil water storage.

656 **Versatility.** The STREAM model is a versatile model suitable for daily runoff and river discharge
657 estimation over sub-basins characterized by different physiographic/climatic characteristics (see e.g.,
658 the outcomes obtained for the gages 9 and 11 located in the driest and wetter part of the Mississippi
659 basin). This aspect is paramount as it gives an insight about the potential of the model to be extended

660 at the global scale. Moreover, the model can be easily adapted to ingest input data with
661 spatial/temporal resolution different from the one tested in this study (0.25°/daily). For instance,
662 satellite missions with higher space/time resolution (e.g., GPM Final Run, ASCAT and NCGM-
663 MAGIC) or near-real time products (e.g., GPM Early Run, EUMETSAT H16, GRACE European
664 Gravity Service for Improved Emergency Management, EGSIM GRACE data [Jäggi et al., 2019](#))
665 could be considered.

666 Additionally, the STREAM model shows highly flexibility as: 1) it can accommodate application
667 domains comprising single or multiple basins of any size; and 2) the sub-catchment delineation
668 procedure can be easily adapted to introduce intermediate outlets along the river in correspondence
669 of gages with available observed river discharge data, useful for model calibration.

670 **Low computational cost.** Due to its simplicity and the limited number of parameters to be calibrated,
671 the computational effort for the STREAM model is very limited (model runs requiring seconds to
672 minutes). For instance, a run of the STREAM model over the presented case study takes less than 2
673 seconds on a machine with 16 GB RAM and 4 Core.

674 However, some limitations have to be acknowledged for the current version of the STREAM model:

675 **Presence of reservoir, diversion, dams or flood plain.** As the STREAM model does not explicitly
676 consider the presence of discontinuity elements along the river network (e. g, reservoir, dam or
677 floodplain), river discharge estimates obtained for gauging stations located downstream of such
678 elements might be inaccurate (see, e.g., gauging stations 1 and 2 in Figure 5).

679 **Snow modelling.** A potential limitation of the current version of the STREAM model is related to
680 the rain/snow differentiation, based on the degree-day coefficient. A different scheme based e.g., on
681 the wet bulb temperature like in IMERG ([Wang et al., 2019](#); [Arabzadeh and Behrangi, 2021](#)), could
682 be investigated in future developments.

683 **Need of in situ data for model calibration and robustness of model parameters.** As discussed in
684 the results section, the parameter values of the STREAM model are set through an automatic
685 calibration procedure aimed at minimizing the differences between modelled and observed river

686 discharge. The main drawbacks of this parameterization technique are a poor predictability of state
687 variables and fluxes at locations and periods not considered in the calibration, and the presence of
688 sharp discontinuities along sub-basin boundaries in state flux and parameter fields (e.g., Merz and
689 Blöschl, 2004). To overcome these issues, several regionalization procedures, as for instance
690 summarized in Cislaghi et al. (2020), could be conveniently applied to transfer model parameters
691 from hydrologically similar catchments to a catchment of interest. In particular, the regionalization
692 of model parameters could allow to, firstly, estimate river discharge and runoff time series over
693 ungauged basins overcoming the need of river discharge data recorded from in-situ networks,
694 secondly, estimate the model parameter values through a physically consistent approach, linking them
695 to the characteristics of the basins and, thirdly, solve the problem of discontinuities in the model
696 parameters, avoiding to obtain patchy unrealistic runoff maps. As this aspect requires additional
697 investigations and it is beyond the paper purpose, it will not be tackled here.

698 **8. CONCLUSIONS**

699 This study presents a new conceptual hydrological model, STREAM, for runoff and river discharge
700 estimation. By using as input satellite data of precipitation, soil moisture and total water storage
701 anomalies, the model has been able to provide accurate daily river discharge and runoff estimates at
702 the outlet river section and the inner river sections and over a $0.25^{\circ} \times 0.25^{\circ}$ spatial grid of the
703 Mississippi river basin. In particular, the model is suitable to reproduce:

- 704 1. river discharge time series over the calibrated river section with good performances both in
705 calibration and validation periods;
- 706 2. river discharge time series over river sections not used for calibration and not located downstream
707 dams or reservoirs;
- 708 3. runoff time series with a quite good agreement with respect to the well-established GRUN
709 observational-based dataset used for comparison.

710 The integration of observations of soil moisture, precipitation and total water storage anomalies is a
711 first alternative method for river discharge and runoff estimation with respect to classical methods
712 based on the use of TWSA-only (suitable for river basins larger than 160'000 km², monthly time
713 scale) or on classical LSMs (Cai et al., 2014).

714 Moreover, although simple, the model has demonstrated a great potential to be easily applied over
715 sub-basins with different climatic and topographic characteristics, suggesting also the possibility to
716 extend its application to other basins. In particular, the analysis over basins with high human impact,
717 where the knowledge of the hydrological cycle and the river discharge monitoring is very important,
718 deserves special attention. Indeed, as the STREAM model is directly ingesting observations of soil
719 moisture and total water storage data, it allows the modeller to neglect processes that are implicitly
720 accounted for in the input data. Therefore, human-driven processes (e.g., irrigation, land use change),
721 that are typically very difficult to model due to missing information and might have a large impact
722 on the hydrological cycle, hence on runoff, could be implicitly modelled. The application of the
723 STREAM model on a larger number of basins with different climatic- physiographic characteristics
724 (e.g., including more arid basins, snow-dominated, lots of topography, heavily managed) along with
725 the results about the sensitivity analysis of the model parameters, will allow to investigate the
726 possibility to regionalize the model parameters and overcome the limitations of the automatic
727 calibration procedure highlighted in the discussion section.

728 **AUTHOR CONTRIBUTION**

729 S.C. performed the analysis and wrote the manuscript. G.G. collected the data and helped in
730 performing the analysis; C.M, L.B., A.T., N.S., H.H.F., C.M., M.R. and J.B. contributed to the
731 supervision of the work. All authors discussed the results and contributed to the final manuscript.

732 **CODE AVAILABILITY**

733 The STREAM model version 1.3, with a short user manual, is freely downloadable in Zenodo
734 (<https://zenodo.org/record/4744984>, doi: 10.5281/zenodo.4744984). The STREAM model code is
735 distributed through M language files, but it could be run with different interpreters of M language,
736 like the GNU Octave (freely downloadable here <https://www.gnu.org/software/octave/download>).

737 **DATA AVAILABILITY**

738 All data and codes used in the study are freely available online. Air temperature data are available at
739 <https://psl.noaa.gov/data/gridded/data.cpc.globaltemp.html> (last access 25/11/202). In situ river
740 discharge data have been taken from the Global Runoff Data Center (GRDC,
741 https://www.bafg.de/GRDC/EN/Home/homepage_node.html (last access 25/11/202). Precipitation
742 and soil moisture data are available from <http://pmm.nasa.gov/data-access/downloads/trmm> and
743 <https://esa-soilmoisture-cci.org/>, respectively.

744 **COMPETING INTERESTS**

745 The authors declare that they have no conflict of interest.

746 **ACKNOWLEDGMENTS**

747 The authors wish to thank the Global Runoff Data Centre (GRDC) for providing most of the
748 streamflow data throughout Europe. The authors gratefully acknowledge support from ESA through
749 the STREAM Project (EO Science for Society element Permanent Open Call contract n°
750 4000126745/19/I-NB).

751

752 **REFERENCE**

- 753 Albergel, C., Rüdiger, C., Carrer, D., Calvet, J. C., Fritz, N., Naeimi, V., Bartalis, Z., and Hasenauer, S.: An evaluation
 754 of ASCAT surface soil moisture products with in-situ observations in southwestern France, *Hydrol. Earth Syst. Sci.*,
 755 13, 115–124, <https://doi.org/doi:10.5194/hess-13-115-2009>, 2009.
- 756 Alcamo, J., Döll, P., Henrichs, T., Kaspar, F., Lehner, B., Rösch, T., & Siebert, S.: Development and testing of the
 757 WaterGAP 2 global model of water use and availability, *Hydrol. Sci. J.*, 48(3), 317-337,
 758 <https://doi.org/10.1623/hysj.48.3.317.45290>, 2003.
- 759 Alexander, J. S., Wilson, R. C., and Green, W. R.: A brief history and summary of the effects of river engineering and
 760 dams on the Mississippi River system and delta (p. 53), US Department of the Interior, US Geological Survey,
 761 <https://doi.org/10.3133/cir1375>, 2012.
- 762 Allen, R.G., Pereira, L. S., Raes, D., and Smith, M: Crop evapotranspiration — guidelines for computing crop water
 763 requirements. FAO Irrigation & Drainage Paper 56. FAO, Rome, 1988.
- 764 Arabzadeh, A., and Behrangi, A.: Investigating Various Products of IMERG for Precipitation Retrieval Over Surfaces
 765 With and Without Snow and Ice Cover, *Remote Sens.*, 13(14), 2726; <https://doi.org/10.3390/rs13142726>, 2021.
- 766 Balsamo, G., A. Beljaars, K. Scipal, P. Viterbo, B. vanden Hurk, M. Hirschi, and A. K. Betts: A revised hydrology for
 767 the ECMWF model: Verification from field site to terrestrial water storage and impact in the integrated forecast
 768 system, *J. Hydrometeorol.*, 10(3), 623–643, <https://doi.org/doi:10.1175/2008JHM1068.1>, 2009.
- 769 Barbarossa, V., Huijbregts, M. A., Beusen, A. H., Beck, H. E., King, H., and Schipper, A. M.: FLO1K, global maps of
 770 mean, maximum and minimum annual streamflow at 1 km resolution from 1960 through 2015, *Scientific Data*,
 771 5, 180052, <https://doi.org/10.1038/sdata.2018.52>, 2018.
- 772 Beck, H. E., van Dijk, A. I., de Roo, A., Dutra, E., Fink, G., Orth, R., and Schellekens, J.: Global evaluation of runoff
 773 from ten state-of-the-art hydrological models, *Hydrol. Earth Syst. Sci.*, 21(6), 2881-2903. <https://doi.org/doi:10.5194/hess-21-2881-2017>, 2017.
- 775 Berghuijs, W. R., Woods, R. A., Hutton, C. J., and Sivapalan, M.: Dominant flood generating mechanisms across the
 776 United States, *Geophys. Res. Lett.*, 43, 4382–4390, <https://doi.org/10.1002/2016GL068070>, 2016.
- 777 Berghuijs, W. R., Woods, R. A., Hutton, C. J., and Sivapalan, M.: Dominant flood generating mechanisms across the
 778 United States, *Geophys. Res. Lett.*, 43, 4382–4390, <https://doi.org/10.1002/2016GL068070>, 2016.
- 779 Bergström, S (1995) The HBV model. In Singh, VP ed. Computer models of watershed hydrology. Water Resources
 780 Publications, Highlands Ranch, CO, 443–476
- 781 Berthet, L., Andréassian, V., Perrin, C., and Javelle, P.: How crucial is it to account for the antecedent moisture conditions
 782 in flood forecasting? Comparison of event-based and continuous approaches on 178 catchments, *Hydrol. Earth Syst.*
 783 *Sci.*, 13(6), 819-831, 2009.
- 784 Blöschl, G., Sivapalan, M., Wagener, T., Viglione, A., and Savenije, H. H. G. (Eds.): Runoff predictions in ungauged
 785 basins: A synthesis across processes, places and scales, Cambridge: Cambridge University Press, 2013.
- 786 Bober, W. Introduction to Numerical and Analytical Methods with MATLAB for Engineers and Scientists; CRC Press,
 787 Inc.: Boca Raton, FL, USA, <https://doi.org/10.1201/b16030>, 2013.
- 788 Botter, G., Peratoner, F., Porporato, A., Rodriguez-Iturbe, I., and Rinaldo, A.: Signatures of large-scale soil moisture
 789 dynamics on streamflow statistics across U.S. Climate regimes, *Water Resour. Res.*, 43, W11413,
 790 <https://doi.org/doi:10.1029/2007WR006162>, 2007b.
- 791 Botter, G., Porporato, A., Daly, E., Rodriguez-Iturbe, I., and Rinaldo, A.: Probabilistic characterization of base flows in
 792 river basins: Roles of soil, vegetation, and geomorphology, *Water Resour. Res.*, 43, W06404,
 793 <https://doi.org/doi:10.1029/2006WR005397>, 2007a.
- 794 Brocca, L., Ciabatta, L., Massari, C., Camici, S., and Tarpanelli, A.: Soil moisture for hydrological applications: open
 795 questions and new opportunities, *Water*, 9(2), 140, <https://doi.org/10.3390/w9020140>, 2017.

796 Brocca, L., Melone, F., and Moramarco, T.: Distributed rainfall-runoff modelling for flood frequency estimation and
797 flood forecasting, *Hydrol. Process.*, 25(18), 2801-2813, <https://doi.org/10.1002/hyp.8042>, 2011.

798 Brocca, L., Melone, F., and Moramarco, T.: On the estimation of antecedent wetness conditions in rainfall-runoff
799 modelling, *Hydrol. Process.*, 22 (5), 629-642, doi:10.1002/hyp.6629. <https://doi.org/10.1002/hyp.6629>, 2008.

800 Brocca, L., Melone, F., Moramarco, T., and Morbidelli, R.: Antecedent wetness conditions based on ERS scatterometer
801 data, *J. Hydrol.*, 364(1-2), 73-87, <https://doi.org/10.1016/j.jhydrol.2008.10.007>, 2009.

802 Cai, X., Yang, Z. L., David, C. H., Niu, G. Y., and Rodell, M.: Hydrological evaluation of the Noah-MP land surface
803 model for the Mississippi River Basin, *J. Geophys. Res. Atmos.*, 119(1), 23-38,
804 <https://doi.org/10.1002/2013JD020792>, 2014.

805 Cislaghi, A., Masseroni, D., Massari, C., Camici, S., and Brocca, L.: Combining a rainfall-runoff model and a
806 regionalization approach for flood and water resource assessment in the western Po Valley, Italy, *Hydrol. Sci. J.*,
807 65(3), 348-370, <https://doi.org/10.1080/02626667.2019.1690656>, 2020.

808 Corradini C, Morbidelli R, Saltalippi C, Melone F. 2002. An adaptive model for flood forecasting on medium size basins.
809 In *Applied Simulation and Modelling*, Ubertini L (ed). IASTED Acta Press: Anaheim (CA); 555-559.

810 Crochemore, L., Isberg, K., Pimentel, R., Pineda, L., Hasan, A., and Arheimer, B.: Lessons learnt from checking the
811 quality of openly accessible river flow data worldwide, *Hydrol. Sci. J.*, 65(5), 699-711,
812 <https://doi.org/10.1080/02626667.2019.1659509>, 2020.

813 Crow, W. T., Bindlish, R., and Jackson, T. J.: The added value of spaceborne passive microwave soil moisture retrievals
814 for forecasting rainfall-runoff partitioning, *Geophys. Res. Lett.*, 32(18), <https://doi.org/10.1029/2005GL023543>,
815 2005.

816 Döll, P., F.Kaspar, and B.Lehner: A global hydrological model for deriving water availability indicators: Model tuning
817 and validation, *J. Hydrol.*, 270(1-2), 105-134, [https://doi.org/doi:10.1016/S0022-1694\(02\)00283-4](https://doi.org/doi:10.1016/S0022-1694(02)00283-4), 2003.

818 Dorigo, W., Wagner, W., Albergel, C., Albrecht, F., Balsamo, G., Brocca, L., Chung, D., Ertl, M., Forkel, M., Gruber, A.,
819 Haas, D., Hamer, P. Hirschi, M., Ikonen, J., de Jeu, R., Kidd, R., Lahoz, W., Liu, Y.Y., Miralles, D., Mistelbauer, T.,
820 Nicolai-Shaw, N., Parinussa, R., Pratola, C., Reimer, C., van der Schalie, R., Seneviratne, S.I., Smolander, T., and
821 Lecomte, P.: ESA CCI Soil Moisture for improved Earth system understanding: state-of-the art and future directions.,
822 *Remote Sens. Environ.*, 203, 185-215, <https://doi.org/10.1016/j.rse.2017.07.001>, 2017.

823 Dyer, J.: Snow depth and streamflow relationships in large North American watersheds, *J. Geophys. Res.*, 113, D18113,
824 <https://doi.org/10.1029/2008JD010031>, 2008.

825 Entekhabi, D., Njoku, E. G., O'Neill, P. E., Kellogg, K. H., Crow, W. T., Edelstein, W. N., ... and Van Zyl, J.: The soil
826 moisture active passive (SMAP) mission. *Proceedings of the Institute of Electrical and Electronics Engineers (IEEE)*,
827 98(5), 704-716. <https://doi.org/doi:10.1109/JPROC.2010.2043918>, 2010.

828 Famiglietti, J. S., and Rodell, M.: Water in the balance, *Science*, 340(6138), 1300-1301,
829 <https://doi.org/10.1126/science.1236460>, 2013.

830 Famiglietti, J.S., and Wood, E. F.: Multiscale modeling of spatially variable water and energy balance processes, *Water*
831 *Resour. Res.*, 30, 3061-3078, <https://doi.org/10.1029/94WR01498>, 1994.

832 Fan, Y. and Van den Dool, H. A: Global monthly land surface air temperature analysis for 1948-present, *J. Geophys.*
833 *Res. Atmos.*, 113, D01103, <https://doi.org/10.1029/2007JD008470>, 2008.

834 Fekete, B. M., Looser, U., Pietroniro, A., and Robarts, R. D.: Rationale for monitoring discharge on the ground, *J.*
835 *Hydrometeorol.*, 13, 1977-1986, <https://doi.org/10.1175/JHM-D-11-0126.1>, 2012.

836 Feldman, A. D. (2000). *Hydrologic modeling system HEC-HMS: technical reference manual*. US Army Corps of
837 Engineers, Hydrologic Engineering Center.

838 Georgakakos KP, and Baumer OW.: Measurement and utilization of onsite soil moisture data, *J. Hydrol.*, 184: , 131-152,
839 [https://doi.org/10.1016/0022-1694\(95\)02971-0](https://doi.org/10.1016/0022-1694(95)02971-0), 1996.

840 Ghiggi, G., Humphrey, V., Seneviratne, S. I., and Gudmundsson, L.: GRUN: an observation-based global gridded runoff
841 dataset from 1902 to 2014, *Earth Syst. Sci. Data*, 11, 1655-1674 *Earth System Science Data*, 11(4), 1655-1674,
842 <https://doi.org/10.5194/essd-11-1655-2019>, 2019.

843 Ghotbi, S., Wang, D., Singh, A., Blöschl, G., and Sivapalan, M.: A New Framework for Exploring Process Controls of
844 Flow Duration Curves, *Water Resour. Res.* *Water Resources Research*, 56(1), <https://doi.org/e2019WR026083>, 2020.

845 Gochis, D. J., Barlage, M., Dugger, A., FitzGerald, K., Karsten, L., McAllister, M., et al. (2018). The WRF-Hydro
846 modeling system technical description, (Version 5.0). NCAR Technical Note. Retrieved from
847 <https://ral.ucar.edu/sites/default/files/public/WRFHydroV5TechnicalDescription.pdf>

848 Gudmundsson, L., and Seneviratne, S. I.: Observation-based gridded runoff estimates for Europe (E-RUN version 1.1),
849 *Earth Syst. Sci. Data*, 8, 279–295, <https://doi.org/10.5194/essd-8-279-2016>, 8(2), 279-2952016, 2016.

850 Gudmundsson, L., Tallaksen, L. M., Stahl, K., Clark, D. B., Du-mont, E., Hagemann, S., Bertrand, N., Gerten, D., Heinke,
851 J., Hanasaki, N., Voss, F., and Koirala, S.: Comparing Large-Scale Hydrological Model Simulations to Observed
852 Runoff Percentiles in Europe, *J. Hydrometeorol.*, 13, 604–62, <https://doi.org/10.1175/JHM-D-11-083.1>, 2012b.

853 Gudmundsson, L., Wagener, T., Tallaksen, L. M., and Engeland, K.: Evaluation of nine large-scale hydrological models
854 with respect to the seasonal runoff climatology in Europe, *Water Resour. Res.*, 48(11),
855 <https://doi.org/10.1029/2011WR010911>, 2012a.

856 Gupta VK, Waymire E, and Wang CT.: A representation of an instantaneous unit hydrograph from geomorphology, *Water*
857 *Resour. Res.*, 16: 855–862, <https://doi.org/doi:10.1029/WR016i005p00855>, 1980.

858 Gupta, H. V., Kling, H., Yilmaz, K. K., and Martinez, G. F.: Decomposition of the mean squared error and NSE
859 performance criteria: Implications for improving hydrological modelling, *J. Hydrol.*, 377(1-2), 80-91,
860 <https://doi.org/10.1016/j.jhydrol.2009.08.003>, 2009.

861 Haddeland, I., Heinke, J., Voß, F., Eisner, S., Chen, C., Hagemann, S., and Ludwig, F.: Effects of climate model radiation,
862 humidity and wind estimates on hydrological simulations, *Hydrol. Earth Syst. Sci.*, 16(2), 305-318,
863 <https://doi.org/10.5194/hess-16-305-2012>, 2012.

864 Hanasaki, N., Kanae, S., Oki, T., Masuda, K., Motoya, K., Shirakawa, N., ... , and Tanaka, K. :An integrated model for
865 the assessment of global water resources–Part 1: Model description and input meteorological forcing, *Hydrol. Earth*
866 *Syst. Sci.*, 12(4), 1007-1025, <https://doi.org/10.5194/hess-12-1007-2008>, 2008.

867 Hastie, T., Tibshirani, R., and Friedman, J. H.: *The Elements of Statistical Learning – Data Mining, Inference, and*
868 *Prediction*, Second Edition, Springer Series in Statistics, Springer, New York, 2nd Edn., available at: [http://www-](http://www-stat.stanford.edu/~tibs/ElemStatLearn/)
869 [stat.stanford.edu/~tibs/ElemStatLearn/](http://www-stat.stanford.edu/~tibs/ElemStatLearn/) (last access: 5 July 2016), 2009.

870 Hong, Y., Adler, R. F., Hossain, F., Curtis, S., and Huffman, G. J.: A first approach to global runoff simulation using
871 satellite rainfall estimation, *Water Resour. Res.*, 43(8), <https://doi.org/10.1029/2006WR005739>, 2007.

872 Horton, R. E.: Hydrological approach to quantitative morphology, *Geol. Soc. Am. Bull.*, 56, 275-370, 1945.

873 Houborg, R., Rodell, M., Li, B., Reichle, R., and Zaitchik, B. F.: Drought indicators based on model-assimilated Gravity
874 Recovery and Climate Experiment (GRACE) terrestrial water storage observations, *Water Resour. Res.*, 48(7),
875 <https://doi.org/10.1029/2011WR011291>, 2012.

876 Hu GR., and Li XY.: Subsurface Flow. In: Li X., Vereecken H. (eds) *Observation and Measurement. Ecohydrology.*
877 Springer, Berlin, Heidelberg. https://doi.org/10.1007/978-3-662-47871-4_9-1, 2018.

878 Huffman, G. J., Adler, R. F., Bolvin, D. T., Gu, G. J., Nelkin, E. J., Bowman, K. P., Hong, Y., Stocker, E. F. and Wolff,
879 D. B.: The TRMM Multisatellite Precipitation Analysis (TMPA): Quasi-Global, Multiyear, Combined-Sensor
880 Precipitation Estimates at Fine Scales, *J. Hydrometeorol.*, 8 (1): 38–55. <https://doi.org/doi:10.1175/jhm560.1>, 2007.

881 Huffman, G. J., Bolvin, D. T., Braithwaite D., Hsu K., Joyce R. , Kidd C., Nelkin Eric J., Sorooshian S., Tan J., and Xie
882 P.: NASA Global Precipitation Measurement (GPM) Integrated Multi-satellitE Retrievals for GPM (IMERG),.
883 https://docsserver.gesdisc.eosdis.nasa.gov/public/project/GPM/IMERG_ATBD_V06.pdf, 2019.

884 Huffman, G. J., Stocker, E. F., Bolvin, D. T., Nelkin, E. J., and Adler, R. F.: TRMM Version 7 3B42 and 3B43 Data Sets.
885 NASA/GSFC, Greenbelt, MD, 2014.

886 Jäggi, A., Weigelt, M., Flechtner, F., Güntner, A., Mayer-Gürr, T., Martinis, S., ... and Shabanloui, A.: European gravity
887 service for improved emergency management (EGSIEM)—from concept to implementation. *Geophysical journal*
888 *international*, 218(3), 1572-1590, 2019, <https://doi.org/10.1093/gji/ggz238>.

889 Kauffeldt, A., Wetterhall, F., Pappenberger, F., Salamon, P., & Thielen, J.: Technical review of large-scale hydrological
890 models for implementation in operational flood forecasting schemes on continental level, *Environ. Model. Softw.*, 75,
891 68-76, <https://doi.org/10.1016/j.envsoft.2015.09.009>, 2016.

892 Kim, H., Watanabe, S., Chang, E. C., Yoshimura, K., Hirabayashi, J., Famiglietti, J., and Oki, T.: Global Soil Wetness
893 Project Phase 3 Atmospheric Boundary Conditions (Experiment 1) [Data set], Data Integration and Analysis System
894 (DIAS), <https://doi.org/10.20783/DIAS.501>, 2017.

895 Kirchner, J. W.: Getting the right answers for the right reasons: Linking measurements, analyses, and models to advance
896 the science of hydrology, *Water Resour. Res.*, 42(3), <https://doi.org/10.1029/2005WR004362>, 2006.

897 Klees, R., Revtova, E. A., Gunter, B.C., Ditmar, P., Oudman, E., Winsemius H. C., and Savenije H.H.G.: The design of
898 an optimal filter for monthly GRACE gravity models, *Geoph. J. Intern.*, 175 (2): 417-432,
899 <https://doi.org/10.1111/j.1365-246X.2008.03922.x>, 2008

900 Kling, H., Fuchs, M., and Paulin, M.: Runoff conditions in the upper Danube basin under an ensemble of climate change
901 scenarios, *J. Hydrol.*, 424, 264-277, <https://doi.org/doi:10.1016/j.jhydrol.2012.01.011>, 2012.

902 Landerer, F. W., and Swenson, S. C.: Accuracy of scaled GRACE terrestrial water storage estimates, *Water Resour. Res.*,
903 48(4), <https://doi.org/10.1029/2011WR011453>, 2012.

904 Lehner, B., C. Reidy Liermann, C. Revenga, C. Vörösmarty, B. Fekete, P. Crouzet, P. Döll, M. Endejan, K. Frenken, J.
905 Magome, C. Nilsson, J.C. Robertson, R. Rodel, N. Sindorf, and D. Wisser.: High-resolution mapping of the world's
906 reservoirs and dams for sustainable river-flow management, *Front. Ecol. Environ.*, 9 (9): 494-502,
907 <https://doi.org/10.1890/100125>, 2011.

908 Lindström, G., Pers, C., Rosberg, J., Strömqvist, J., & Arheimer, B.: Development and testing of the HYPE (Hydrological
909 Predictions for the Environment) water quality model for different spatial scales, *Hydrol. Res.*, 41(3-4), 295-319,
910 <https://doi.org/10.2166/nh.2010.007>, 2010.

911 Long, D., Longuevergne, L., and Scanlon, B. R.: Uncertainty in evapotranspiration from land surface modeling, remote
912 sensing, and GRACE satellites, *Water Resour. Res.*, 50(2), 1131-1151, <https://doi.org/10.1002/2013WR014581>,
913 2014.

914 Lorenz, C., H. Kunstmann, H., B. Devaraju, B., Tourian, M. J., N. Sneeuw, N., and J. Riegger, J.: Large-Scale Runoff
915 from Landmasses: A Global Assessment of the Closure of the Hydrological and Atmospheric Water Balances., *J.*
916 *Hydrometeor.*, 15, 2111-2139, <https://doi.org/doi:10.1175/JHM-D-13-0157.1>, 2014.

917 Luthcke, S.B., Sabaka, T.J., Loomis, B.D., Arendt, A.A., McCarthy, J.J., and Camp, J.: Antarctica, Greenland and Gulf
918 of Alaska land-ice evolution from an iterated GRACE global mascon solution, *J. Glaciol.*, Vol. 59, No. 216, 613-631,
919 2013 <https://doi.org/doi:10.3189/2013JoG12J147>, 2013.

920 Markstrom, S.L., Regan, R.S., Hay, L.E., Viger, R.J., Webb, R.M.T., Payn, R.A., and LaFontaine, J.H.: PRMS-IV, the
921 precipitation-runoff modeling system, version 4: U.S. Geological Survey Techniques and Methods, book 6, chap. B7,
922 158 p., <https://doi.org/10.3133/tm6B7>, 2015

923 Massari, C., Brocca, L., Barbetta, S., Papathanasiou, C., Mimikou, M., and Moramarco, T.: Using globally available soil
924 moisture indicators for flood modelling in Mediterranean catchments, *Hydrol. Earth Syst. Sci.*, 18(2), 839,
925 <https://doi.org/10.5194/hess-18-839-2014>, 2014.

926 Massari, C., Brocca, L., Barbetta, S., Papathanasiou, C., Mimikou, M., and Moramarco, T.: Using globally available soil
927 moisture indicators for flood modelling in Mediterranean catchments, *Hydrol. Earth Syst. Sci.*, 18(2), 839,
928 <https://doi.org/10.5194/hess-18-839-2014>, 2014.

929 Massari, C., Brocca, L., Tarpanelli, A., Hong, Y., Crow, W., Ciabatta, L., Camici, S., Barbetta, S., and Moramarco, T.:
930 Global surface runoff estimation in near real time by using SMAP and GPM, poster at SMAP conference, 2016.

931 Massari, C., Brocca, L., Tarpanelli, A., Hong, Y., Crow, W., Ciabatta, L., Camici, S., Barbetta, S., and Moramarco, T.:
932 Global surface runoff estimation in near real time by using SMAP and GPM, poster at SMAP conference, 2016.

933 Massotti, L., Siemes, C., March, G., Haagmans, R., and Silvestrin, P.: Next generation gravity mission elements of the
934 mass change and geoscience international constellation: From orbit selection to instrument and mission
935 design. *Remote Sensing*, 13(19), 3935. <https://doi.org/10.3390/rs13193935>, 2021.

936 Maxwell, R. M., Condon, L. E., and Kollet, S. J.: A high-resolution simulation of groundwater and surface water over
937 most of the continental US with the integrated hydrologic model ParFlow v3, *Geosci. Model Dev.*, 8, 923–937,
938 <https://doi.org/10.5194/gmd-8-923-2015>, 2015.

939 Maxwell, R. M., Condon, L. E., and Kollet, S. J.: A high-resolution simulation of groundwater and surface water over
940 most of the continental US with the integrated hydrologic model ParFlow v3, *Geosci. Model Dev.*, 8, 923–937,
941 <https://doi.org/10.5194/gmd-8-923-2015>, 2015.

942 Merz, R., and Blöschl, G.: A regional analysis of event runoff coefficients with respect to climate and catchment
943 characteristics in Austria, *Water Resour. Res.*, 45(1), <https://doi.org/10.1029/2008WR007163>, 2009.

944 Mueller Schmied, H., Adam, L., Eisner, S., Fink, G., Flörke, M., Kim, H., ... and Song, Q.: Variations of global and
945 continental water balance components as impacted by climate forcing uncertainty and human water use, *Hydrol. Earth
946 Syst. Sci.*, 20(7), 2877-2898, <https://doi.org/10.5194/hess-20-2877-2016>, 2016.

947 Muneeppeerakul, R., Azaele, S., Botter, G., Rinaldo, A., and Rodriguez-Iturbe, I.: Daily streamflow analysis based on a
948 two-scaled gamma pulse model, *Water Resour. Res.*, 46(11), <https://doi.org/10.1029/2010WR009286>, 2010.

949 Nash, J. E.: The form of the instantaneous unit hydrograph, IASH publication no. 45, 3–4, 114–121, 1957.

950 Natural Resources Conservation Service (NRCS): Urban hydrology for small watersheds, Tech. Release 55, 2nd ed., U.S.
951 Dep. of Agric., Washington, D. C. (available at [ftp://ftp.wcc.nrcs.usda.gov/downloads/
952 hydrology_hydraulics/tr55/tr55.pdf](ftp://ftp.wcc.nrcs.usda.gov/downloads/hydrology_hydraulics/tr55/tr55.pdf)), 1986.

953 Noacco, V., Sarrazin, F., Pianosi, F., & Wagener, T.: Matlab/R workflows to assess critical choices in Global Sensitivity
954 Analysis using the SAFE toolbox. *MethodsX*, 6, 2258-2280, 2019, <https://doi.org/10.1016/j.mex.2019.09.033>.

955 Oleson, K., Lawrence, D. M., Bonan, G. B., Drewniak, B., Huang, M., Koven, C. D., ... Yang, Z. -L.: Technical
956 description of version 4.5 of the Community Land Model (CLM) (No. NCAR/TN-503+STR).
957 <http://dx.doi.org/10.5065/D6RR1W7M>, 2013.

958 Orth, R., and Seneviratne, S. I.: Introduction of a simple-model-based land surface dataset for Europe, *Environ. Res. Lett.*,
959 10(4), 044012, <https://doi.org/10.1088/1748-9326/10/4/044012>, 2015.

960 Pellet, V., Aires, F., Munier, S., Fernández Prieto, D., Jordá, G., Dorigo, W. A., ... and Brocca, L.: Integrating multiple
961 satellite observations into a coherent dataset to monitor the full water cycle—application to the Mediterranean region.,
962 *Hydrol. Earth Syst. Sci.*, 23(1), 465-491, <https://doi.org/10.5194/hess-23-465-2019>, 2019.

963 Pianosi, F., Sarrazin, F., Wagener, T. (2015), A Matlab toolbox for Global Sensitivity Analysis, *Environmental Modelling
964 & Software*, 70, 80-85, <https://doi.org/10.1016/j.envsoft.2015.04.009>.

965 Prudhomme, C., Giuntoli, I., Robinson, E. L., Clark, D. B., Arnell, N. W., Dankers, R., ... and Hagemann, S.: Hydrological
966 droughts in the 21st century, hotspots and uncertainties from a global multimodel ensemble experiment, *Proceedings
967 of the National Academy of Sciences*, 111(9), 3262-3267, 2014.

968 Rakovec, O., Kumar, R., Attinger, S., and Samaniego, L.: Improving the realism of hydrologic model functioning through
969 multivariate parameter estimation, *Water Resour. Res.*, 52(10), 7779-7792, <https://doi.org/10.1002/2016WR019430>,
970 2016.

971 Riegger, J., and Tourian, M. J.: Characterization of runoff-storage relationships by satellite gravimetry and remote
972 sensing, *Water Resour. Res.*, 50, 3444–3466, <https://doi.org/doi:10.1002/2013WR013847>, 2014.

973 Rodell, M., Beaudoin, H. K., L’Ecuyer, T. S., Olson, W. S., Famiglietti, J. S., Houser, P. R., Adler, R., Bosilovich, M.
974 G., Clayson, C. A., Chambers, D., Clark, E., Fetzer, E. J., Gao, X., Gu, G., Hilburn, K., Huffman, G. J., Lettenmaier,
975 D. P., Liu, W. T., Robertson, F. R., Schlosser, C. A., Sheffield, J. and Wood, E. F.: The observed state of the water
976 cycle in the early 15twenty-first century, *J. Clim.*, 28(21), 8289–8318, [https://doi.org/doi:10.1175/JCLI-D-14-
977 00555.1](https://doi.org/doi:10.1175/JCLI-D-14-

977 00555.1), 2015.

978 Schellekens, J., Dutra, E., Martínez-de la Torre, A., Balsamo, G., van Dijk, A., Sperna Weiland, F., Minvielle, M., Cal-
979 vet, J.-C., Decharme, B., Eisner, S., Fink, G., Flörke, M., Peßenteiner, S., van Beek, R., Polcher, J., Beck, H., Orth, R.,
980 Calton, B., Burke, S., Dorigo, W., and Weedon, G. P.: A global water resources ensemble of hydrological models: the
981 earth2Observe Tier-1 dataset, *Earth Syst. Sci. Data*, 9, 389–413, <https://doi.org/10.5194/essd-9-389-2017>, 2017.

- 982 Schwanghart, W., and Kuhn, N. J.: TopoToolbox: A set of Matlab functions for topographic analysis., Environ. Model.
983 Softw.Environmental Modelling & Software, 25(6), 770-781, 2010.
- 984 Seneviratne, S. I., Corti, T., Davin, E. L., Hirschi, M., Jaeger, E. B., Lehner, I., ... and Teuling, A. J.: Investigating soil
985 moisture–climate interactions in a changing climate: A review, Earth-Sci. Rev., 99(3-4), 125-161,
986 <https://doi.org/10.1016/j.earscirev.2010.02.004>, 2010.
- 987 Sneeuw, N., Lorenz, C., Devaraju, B., Tourian, M. J., Riegger, J., Kunstmann, H., and Bárdossy, A.: Estimating runoff
988 using hydro-geodetic approaches, Surv. Geophys, 35(6), 1333-1359, <https://doi.org/10.1007/s10712-014-9300-4>,
989 2014.
- 990 Sobol, I.M. (1993), Sensitivity analysis for non-linear mathematical models, Math. Model. Comput. Exp. Transl. Russ.
991 IM Sobol' Sensit. Estim. Nonlinear Math. Models Mat. Model. 2, 1 (4) (1993), pp. 407-414, 1990 112–118.
- 992 Solomatine, D. P., and Ostfeld, A.: Data-driven modelling: some past experiences and new approaches, J. Hydroinform.,
993 10(1), 3-22, <https://doi.org/10.2166/hydro.2008.015>, 2008.
- 994 Sood, A., and Smakhtin, V.: Global hydrological models: a review, Hydrol. Sci. J., 60(4), 549-565,
995 <https://doi.org/10.1080/02626667.2014.950580>, 2015.
- 996 Strahler, A. N.: Hypsometric (area-altitude) analysis of erosional topography, Geol. Soc. Am. Bull.Geological Society of
997 America Bulletin, 63(11), 1117-1142, [https://doi.org/10.1130/0016-7606\(1952\)63\[1117:HAAOET\]2.0.CO;2](https://doi.org/10.1130/0016-7606(1952)63[1117:HAAOET]2.0.CO;2), 1952.
- 998 Tang, Y., Reed, P., Wagener, T. and Van Werkhoven, K. Comparing sensitivity analysis methods to advance lumped
999 watershed model identification and evaluation. Hydrology & Earth System Sciences 11, 793–817, 2007.
- 1000 Tapley, B.D., Watkins, M.M., Flechtner, F. et al.: Contributions of GRACE to understanding climate change, Nat. Clim.
1001 Chang., 9, 358–369, <https://doi.org/doi:10.1038/s41558-019-0456-2>, 2019.
- 1002 Thiemig, V., Rojas, R., Zambrano-Bigiarini, M., and De Roo, A.: Hydrological evaluation of satellite rainfall estimates
1003 over the Volta and Baro-Akobo Basin, J. Hydrol., 499, 324-338, <https://doi.org/10.1016/j.jhydrol.2013.07.012>, 2013.
- 1004 Thornthwaite C.W., 1948. An approach toward a rational classification of climate. Geogr. Rev., 38, 55-94.
- 1005 Tourian, M. J., Reager, J. T., and Sneeuw, N.: The total drainable water storage of the Amazon river basin: A first estimate
1006 using GRACE, Water Resour. Res., 54., <https://doi.org/10.1029/2017WR021674>, 2018.
- 1007 Trambly, Y., Bouvier, C., Martin, C., Didon-Lescot, J. F., Todorovik, D., and Domergue, J. M.: Assessment of initial
1008 soil moisture conditions for event-based rainfall–runoff modelling, J. Hydrol., 387(3-4), 176-187,
1009 <https://doi.org/10.1016/j.jhydrol.2010.04.006>, 2010.
- 1010 Troutman, B. M., and Karlinger, M.B.: Unit hydrograph approximation assuming linear flow through topologically
1011 random channel networks, Water Resour. Res., 21.; 743 – 754, <https://doi.org/doi:10.1029/WR021i005p00743>, 1985.
- 1012 Van Beek, L. P. H., and Bierkens, M. F. P.: The global hydrological model PCR-GLOBWB: conceptualization,
1013 parameterization and verification. Utrecht University, Utrecht, The Netherlands, 1, 25-26, 2009.
- 1014 Vishwakarma, B. D., Devaraju, B., and Sneeuw, N.: What is the spatial resolution of GRACE satellite products for
1015 hydrology?, Remote Sensing, 10, 852, <https://doi.org/10.3390/rs10000852>, 2018.
- 1016 Vörösmarty C. J., and Coauthors: Global water data: A newly endangered species, Eos, Trans. Amer. Geophys. Union,
1017 82, 54, <https://doi.org/10.1029/01EO00031>, 2002.
- 1018 Vose, R.S., Applequist, S., Durre, I., Menne, M.J., Williams, C.N., Fenimore, C., Gleason, K., and Arndt, D.: Improved
1019 Historical Temperature and Precipitation on Time Series For U.S. Climate Divisions., J. Meteorol. and Climat.,
1020 53(May), 1232–1251., <https://doi.org/10.1175/JAMC-D-13-0248.1> DOI: 10.1175/JAMC-D-13-0248.1, 2014.
- 1021 Wagner, W., Blöschl, G., Pampaloni, P., Calvet, J. C., Bizzarri, B., Wigneron, J. P., and Kerr, Y.: Operational readiness
1022 of microwave remote sensing of soil moisture for hydrologic applications, Hydrol. Res., 38(1), 1-20,
1023 <https://doi.org/10.2166/nh.2007.029>, 2007.
- 1024 Wagner, W., Lemoine, G., and Rott, H.: A method for estimating soil moisture from ERS scatterometer and soil data.,
1025 Remote Sens. Environ.Remote Sensing of Environment, 70, 191–207, [https://doi.org/doi:10.1016/S0034-4257\(99\)00036-X](https://doi.org/doi:10.1016/S0034-4257(99)00036-X), 1999.
- 1026

- 1027 Wang, Y. H., Broxton, P., Fang, Y., Behrangi, A., Barlage, M., Zeng, X., and Niu, G. Y.: A wet-bulb temperature-based
1028 rain-snow partitioning scheme improves snowpack prediction over the drier western United States, *Geophys. Res.*
1029 *Lett.*, 46(23), 13825-13835, <https://doi.org/10.1029/2019GL085722>, 2019.
- 1030 Wisser, D., Fekete, B. M., Vörösmarty, C. J., and Schumann, A. H.: Reconstructing 20th century global hydrography: a
1031 contribution to the Global Terrestrial Network- Hydrology (GTN-H), *Hydrol. Earth Syst. Sci.*, 14, 1–24,
1032 <https://doi.org/doi:10.5194/hess-14-1-2010>, 2010.
- 1033 Yokoo, Y., and Sivapalan, M.: Towards reconstruction of the flow duration curve: Development of a conceptual
1034 framework with a physical basis, *Hydrol. Earth Syst. Sci.*, 15(9), 2805–2819, [https://doi.org/10.5194/hess-15-2805-](https://doi.org/10.5194/hess-15-2805-2011)
1035 2011, 2011.
- 1036 Zhang, Y., Pan, M., Sheffield, J., Siemann, A. L., Fisher, C. K., Liang, M., ... and Zhou, T.: A Climate Data Record
1037 (CDR) for the global terrestrial water budget: 1984–2010, *Hydrol. Earth Syst. Sci.*, 22, 241–263,
1038 [https://doi.org/10.5194/hess-22-241-2018\(Online\)](https://doi.org/10.5194/hess-22-241-2018(Online)), 22(PNNL-SA-129750), 2018.
- 1039

1040 Table 1. Location of river discharge gauging stations over the Mississippi basins and upstream
 1041 contributing area. Bold text is used to indicate gages where the STREAM model has been calibrated.

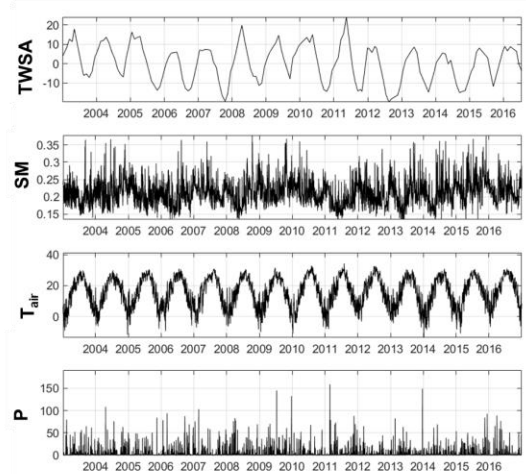
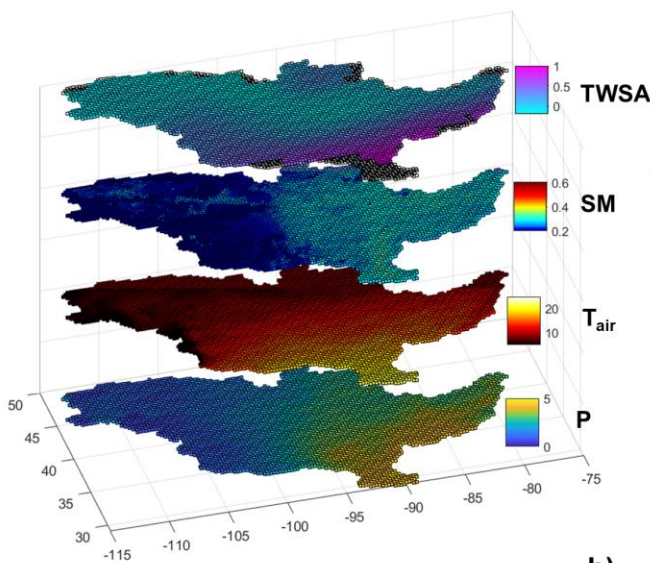
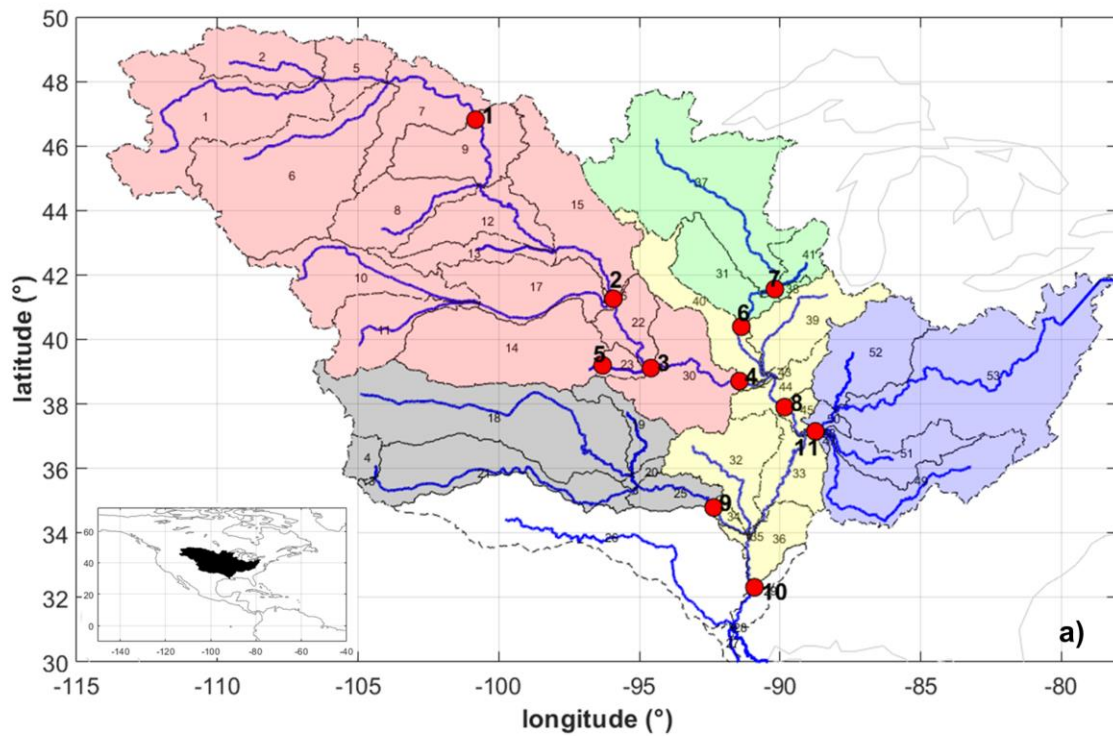
#	River	Gage name	Latitude (°)	Longitude (°)	Upstream area (km ²)	Mean annual river discharge (m ³ /s)	Presence of dam
1	Missouri	Bismarck, ND	-100.82	46.81	481232	633	Garrison dam
2	Missouri	Omaha, NE	-95.92	41.26	814371	914	Gavins Point Dam
3	Missouri	Kansas City, MO	-94.59	39.11	1229427	1499	---
4	Missouri	Hermann, MO	-91.44	38.71	1330000	2326	---
5	Kansas	Wamego, KS	-96.30	39.20	143054	141	Kanopolis
6	Mississippi	Keokuk, IA	-91.37	40.39	282559	1948	---
7	Rock	Near Joslin, IL	-90.18	41.56	23835	199	---
8	Mississippi	Chester, IL	-89.84	37.90	1776221	6018	---
9	Arkansas	Murray Dam Near Little Rock, AR	-92.36	34.79	408068	1249	---
10	Mississippi	Vicksburg, MS	-90.91	32.32	2866590	17487	---
11	Ohio	Metropolis, ILL.	-88.74	37.15	496134	7931	---

1042
 1043

1044 Table 2. Performance scores obtained over the Mississippi river gauging stations during the
 1045 calibration and validation periods.

#	CALIBRATION PERIOD			VALIDATION PERIOD		
SCORE	<i>KGE</i> (-)	rho (-)	<i>RRMSE</i> (%)	<i>KGE</i> (-)	rho (-)	<i>RRMSE</i> (%)
GAUGING STATIONS USED FOR CALIBRATION						
10	0.78	0.78	30	0.71	0.80	40
9	0.79	0.80	66	0.21	0.90	112
6	0.80	0.80	42	0.74	0.81	48
4	0.78	0.78	45	0.73	0.76	49
11	0.80	0.81	45	0.72	0.85	51
GAUGING STATIONS NOT USED FOR CALIBRATION						
1	-3.07	0.09	131	0.43	0.45	93
2	-0.46	0.50	110	0.44	0.54	86
3	0.23	0.73	78	0.42	0.72	69
5	-1.43	0.24	361	-1.23	0.31	355
7	0.55	0.62	72	0.34	0.64	76
8	0.81	0.84	35	0.78	0.83	39

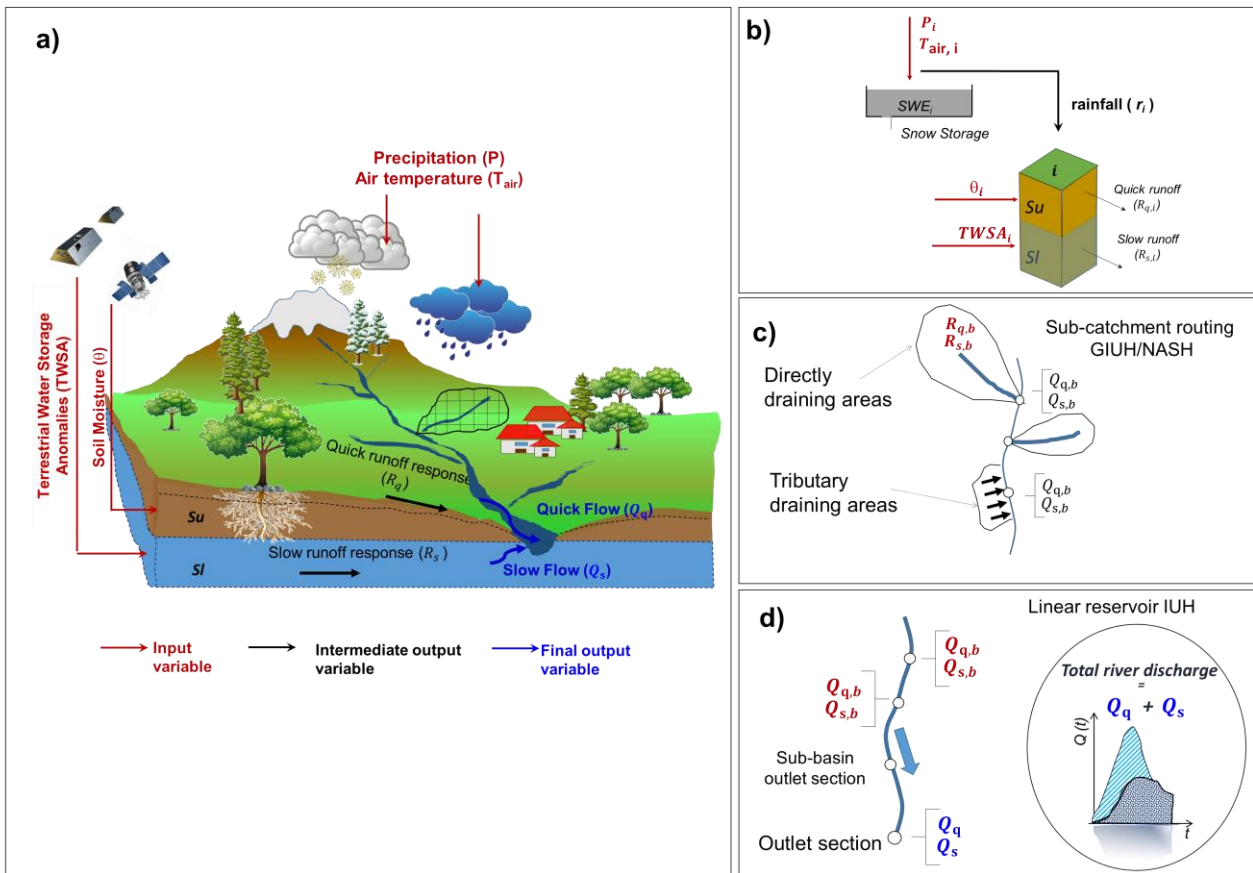
1046
 1047



1048

1049 Figure 1. Mississippi river basin. Figure 1a) illustrates the sub-catchments delineation. The black
 1050 dashed lines and the numbers in the map identify the 53 sub-catchments (tributary and directly
 1051 draining areas) in the Mississippi basin, blue lines represent the mainstem of each sub-catchment.
 1052 Red dots indicate the location of the river discharge gauging stations; different colours identify
 1053 different inner cross-sections (and the related contributing sub-catchments) used for the model
 1054 calibration. Figure 1b) shows the gridded mean daily values of the input data for the period 2003-
 1055 2016. Figure 1c) illustrates the input time series over a point located inside the basin.

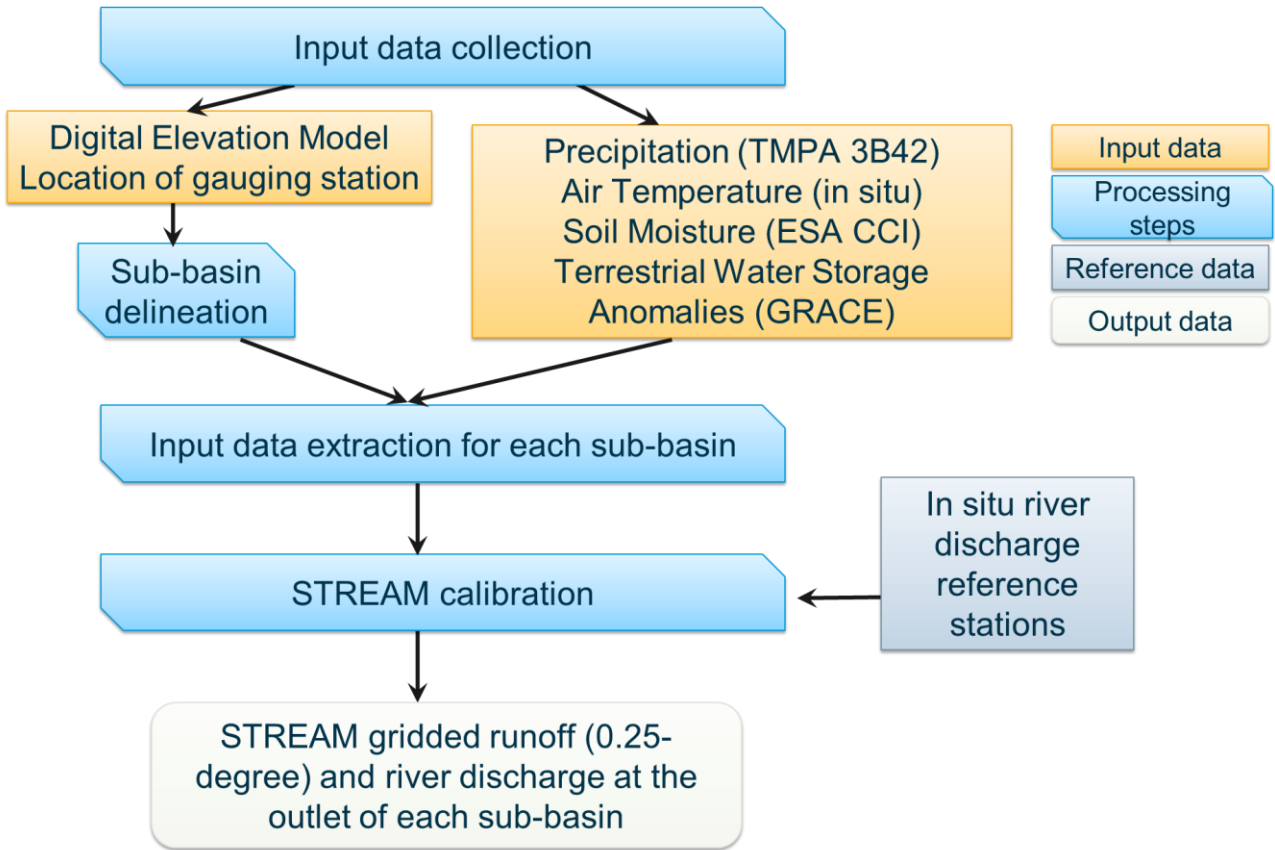
1056
 1057
 1058



1059
 1060
 1061
 1062
 1063
 1064
 1065
 1066
 1067

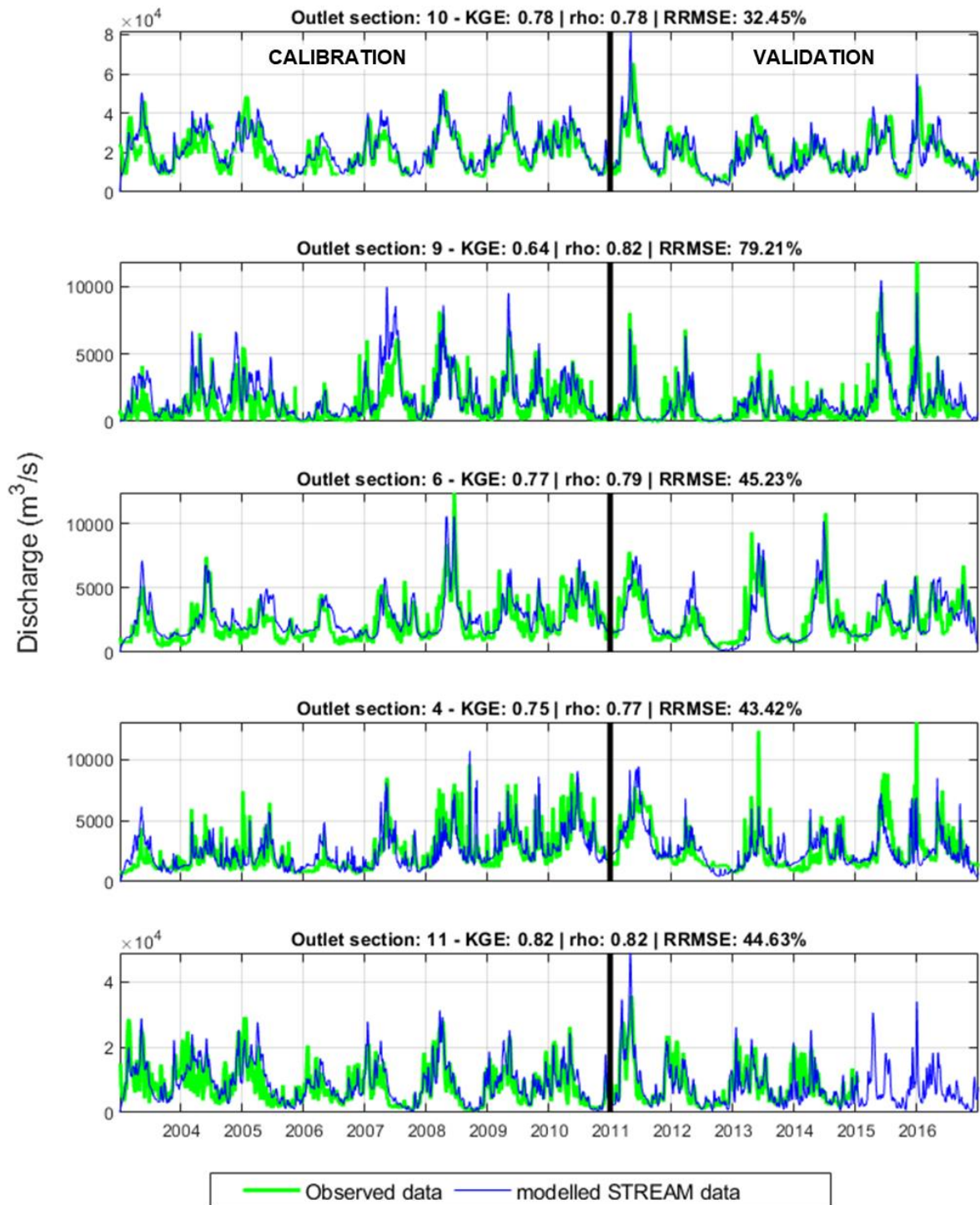
Figure 2. Configuration of the STREAM model adopted for runoff and river discharge estimation. Figure 2a) gives an overview of the needed input data and the variables can be obtained as model output. Figure 2b) illustrates the runoff generation at cell scale. Figure 2c) refers to the sub-catchment river discharge calculation and Figure 2d) illustrates the river discharge routing through river networks. Red arrows indicate input variables; black arrows indicate intermediate output variables; blue arrows indicate final output variables. Please refer to text for symbols.

1068



1069
1070
1071
1072

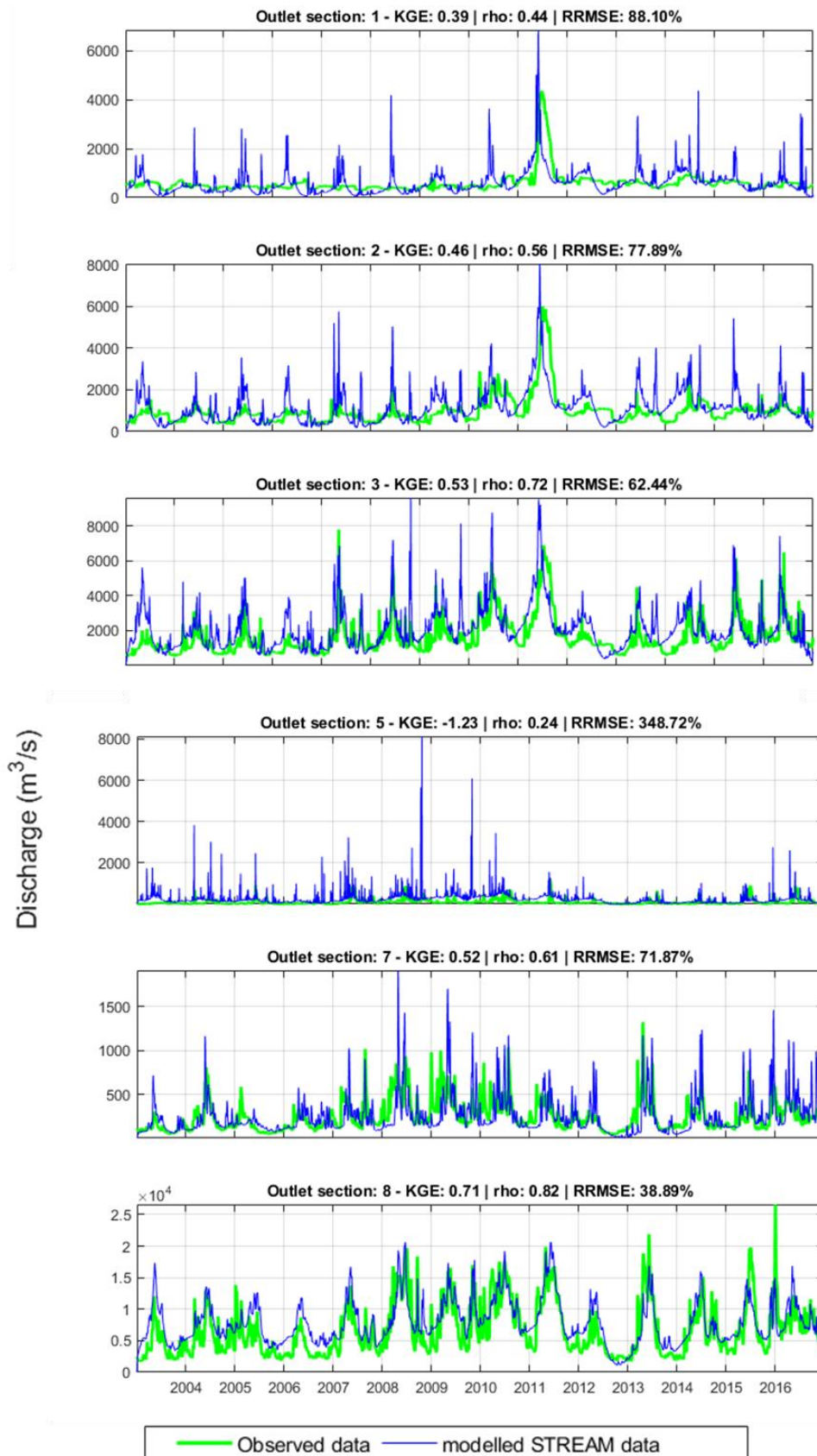
Figure 3. Processing steps of the STREAM model.



1073

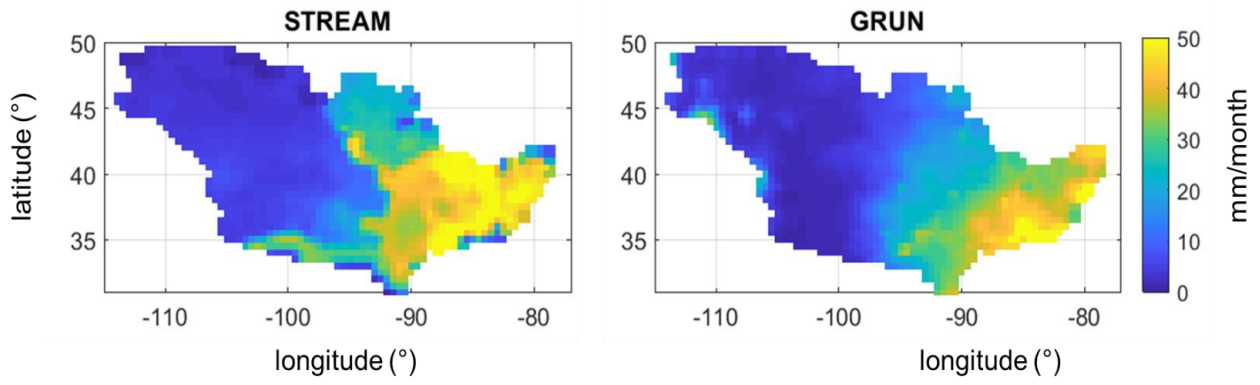
1074 Figure 4. Comparison between observed and modelled river discharge time series over the five
 1075 calibrated sections in the Mississippi river basin. Performance scores at the top of each plot refer to
 1076 the entire study period (2003–2016).

1077



1070
 1081
 1082
 1083
 1084

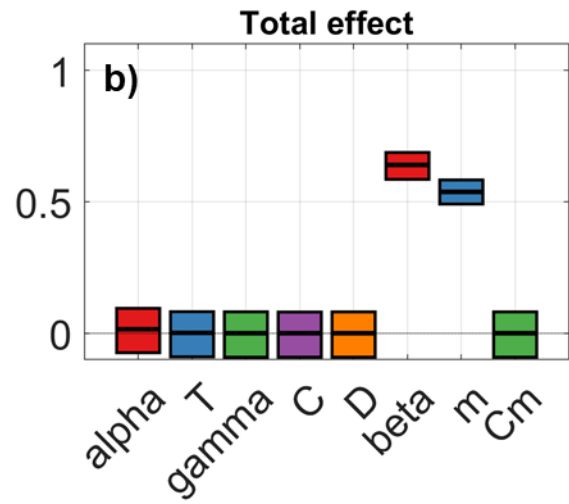
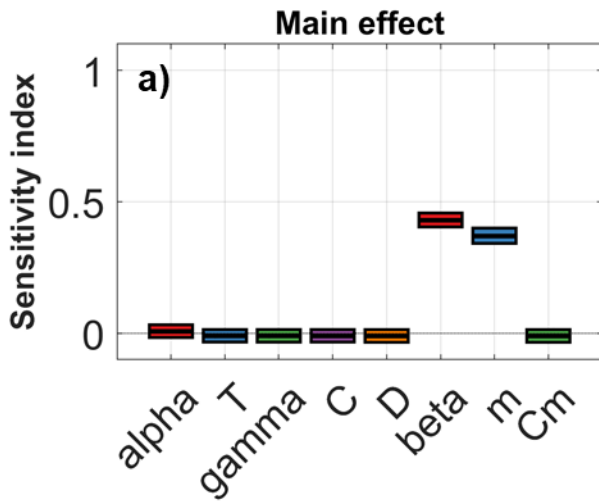
Figure 5. Comparison between observed and modelled river discharge time series over the gauged sections not used in the calibration phase. Performance scores at the top of each plot refer to the entire study period (2003–2016).



1085

1086 Figure 6. Mississippi river basin: mean monthly runoff for the period 2003–2014 obtained by
1087 STREAM and GRUN models.

1088



1089
 1090
 1091
 1092
 1093
 1094

Figure 7. Main effect a) and total effect b) sensitivity indices calculated using the VBSA method for Vicksburg gauging station. The boxes represent the 95% bootstrap confidence intervals and the central black lines indicate the bootstrap mean.

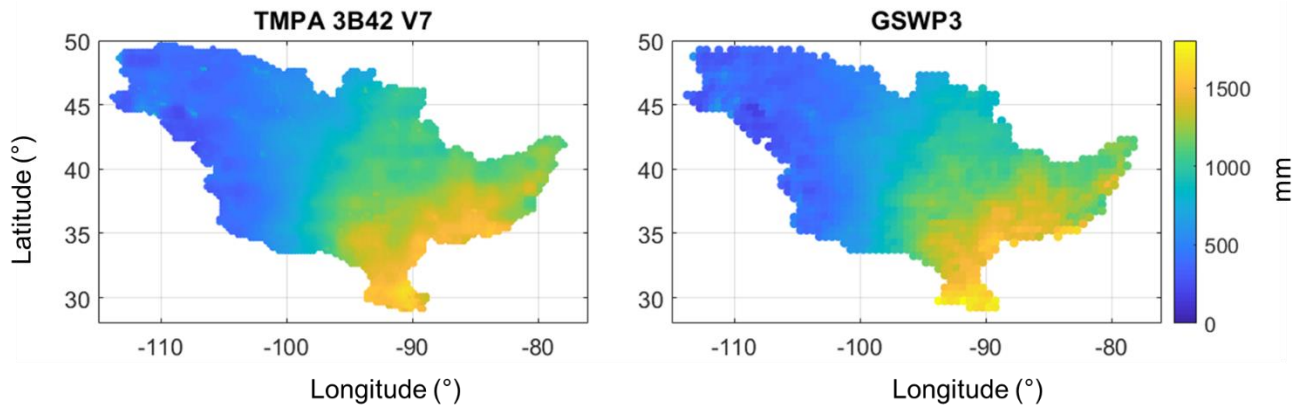
1095 **APPENDIX**

1096 Table 1A. Description of STREAM parameters, belonging module, variability range and unit.

Parameter	Description	Module	Range Variability	Unit
Cm	degree-day coefficient	Snow	0.1/24-3	[-]
α	exponent of infiltration	Soil	1-30	[-]
T	characteristic time length	Soil	0.01-80	[days]
β	coefficient relationship <i>slow-flow</i> runoff component and TWSA	Soil	0.1-20	[mm h ⁻¹]
m	exponent in the relationship between <i>slow-flow</i> runoff component and TWSA	Soil	1-15	[-]
γ	parameter of GIUH	Routing	0.5-5.5	[-]
C	Celerity	Routing	1-60	[km h ⁻¹]
D	Diffusivity	Routing	1-30	[km ² h ⁻¹]

1097

1098



1099

1100 Figure A1. Mean annual precipitation data over the period 2003-2014 obtained by TMPA 3B42 V7
1101 and GSWP3 datasets over the Mississippi river basin.

1102